Exposure of five cementitious sealant materials to wet supercritical CO2 and CO2-saturated water under simulated downhole conditions

van Noort, Reinier; Svenningsen, Gaute; Li, Kai; Pluymakers, Anne

DOI
10.1016/j.ijggc.2025.104380

Publication date
2025

Document Version
Final published version

Published in
International Journal of Greenhouse Gas Control

Citation (APA)
van Noort, R., Svenningsen, G., Li, K., & Pluymakers, A. (2025). Exposure of five cementitious sealant materials to wet supercritical CO2 and CO2-saturated water under simulated downhole conditions. *International Journal of Greenhouse Gas Control*, *144*, Article 104380. https://doi.org/10.1016/j.ijggc.2025.104380

International Journal of Greenhouse Gas Control 144 (2025) 104380

Contents lists available at ScienceDirect

International Journal of Greenhouse Gas Control

journal homepage: www.elsevier.com/locate/ijggc

Exposure of five cementitious sealant materials to wet supercritical CO_2 and CO_2-saturated water under simulated downhole conditions

Reinier van Noort [a,*], Gaute Svenningsen [a], Kai Li [b,c], Anne Pluymakers [b]

[a] Institute for Energy Technology, Instituttveien 18, 2007, Kjeller, Norway
[b] Geoscience & Engineering Department, Delft University of Technology, Delft, the Netherlands
[c] Geothermal Energy & Reservoir Technology, Karlsruhe Institute of Technology, Karlsruhe, Germany

ARTICLE INFO

Keywords:
CCS
Geological CO_2 storage
Wellbore integrity
Wellbore sealant
Cement
Sealant
Integrity
Storage integrity
Geopolymer

ABSTRACT

Maintaining well integrity is a key challenge to the secure geological storage of CO_2. Here, sealants based on Portland Cement form a key component, providing seals between the steel wellbore and surrounding caprock, as well as plugs for sealing wells that will no longer be used. However, exposure of sealants based on Portland Cement to CO_2-bearing fluids may lead to carbonation, potentially followed by degradation of these materials during prolonged exposure or flow, which may thus negatively impact well integrity. Therefore, new sealant materials need to be developed to help ensure long-term well integrity.

This paper reports exposure of five different sealants to CO_2-saturated water and wet supercritical CO_2 at in-situ conditions (80 °C and 10 MPa). Three of the sealants investigated are based on Portland Cement, while the other two are based on Calcium Aluminate Cement, and a rock-based geopolymer specifically developed for Geological CO_2 Storage (GCS). The five sealants were selected to represent different methods for improving wellbore seal integrity, such as restricting permeability (and porosity), or modifying how the material interacts with CO_2-bearing fluids. Exposures were carried out in a purpose-built batch apparatus, enabling simultaneous exposure of up to 10 samples in total to CO_2-saturated water and wet supercritical CO_2.

After exposure, changes in the sealants' microstructures and chemical and mineralogical compositions were assessed using scanning electron microscopy with energy-dispersive X-ray spectroscopy, computed tomography scanning, and fluid chemical analysis. The impact of exposure to CO_2-bearing fluids was interpreted in terms of alteration and degradation of the materials, to compare how different sealant design modifications can be employed to enhance wellbore integrity.

1. Introduction

The underground storage of captured CO_2, (Geological CO_2 Storage – GCS) as part of Carbon Capture and Storage (CCS), is of key importance for achieving the climate goals set in the Paris Agreement (cf. UNFCCC, 2015; IPCC, 2022). In such geological carbon storage, the sealants used as annular wellbore seals and as plugs in wellbores that are abandoned have been identified as potential points of weakness where leakages may develop. Such leakages may form already during emplacement of the seal; during (periodic) CO_2-injection; or during the long subsequent storage period. They may develop through the sealant body, along (pre-existing) cracks, and along the contacts between sealant and steel wellbore, or sealant and host rock; and this may occur due to chemical, mechanical and/or thermal effects (cf. Carroll et al., 2016; Celia et al., 2005; Zhang and Bachu, 2011).

The impact of CO_2-exposure on cements used as wellbore seals has been studied experimentally (Abid et al., 2015; Barlet-Gouédard et al., 2006; Bjørge et al., 2019; Chavez Panduro et al., 2017; Duguid, 2009; Duguid and Scherer, 2010; Gu et al., 2017; IEAGHG, 2011; Jacquemet et al., 2012, 2008; Kutchko et al., 2015, 2007, 2011; Kutchko et al., 2009, 2008; Laudet et al., 2011; Lende et al., 2021; Lesti et al., 2013; Liteanu and Spiers, 2011; Matteo and Scherer, 2012; Omosebi et al., 2015; Sterpenich et al., 2014; Todorovic et al., 2020; Wigand et al., 2009; Zhang et al., 2014a, 2014b), numerically (Brunet et al., 2013; Hernández-Rodríguez et al., 2017; Jacquemet et al., 2012; Walsh et al., 2014; Xiao et al., 2017), and on cement samples retrieved from wells that were exposed to CO_2 (Carey et al., 2007; Crow et al., 2009). Experimental studies have mostly been conducted by batch-exposure of

* Corresponding author.
E-mail address: Reinier@ife.no (R. van Noort).

https://doi.org/10.1016/j.ijggc.2025.104380
Received 15 July 2024; Received in revised form 14 March 2025; Accepted 11 April 2025
Available online 17 April 2025

cured cement samples, exposing such samples to CO_2-saturated water or brine, or, less commonly, directly to a water-saturated CO_2-phase (Lende et al., 2021). Alternatively, cured sealant cylinders can be exposed using a flow-through method, where a flow of CO_2-saturated water or supercritical CO_2 is forced through a sample under an exaggerated pressure gradient, though such tests are not carried out as commonly due to the laboratory equipment required, and relative complexity of setting up and running such tests (cf. Laudet et al., 2011; Lende et al., 2021). Typically, tests exposing sealants based on Ordinary Portland Cement (OPC) to CO_2-saturated water show that such exposure leads to the dissolution of free portlandite ($Ca(OH)_2$), followed by the leaching of Ca^{2+} from Calcium-Silicates-Hydrates (CSH). This Ca^{2+} then precipitates locally or outside the sample as initially stable $CaCO_3$. Precipitation of carbonates within the cement matrix can lead to a decrease in porosity (and permeability), and potentially an enhancement of mechanical properties, and carbonate precipitation may even fill annuli, fractures, and similar leakage pathways, healing damaged cement seals (Abdoulghafour et al., 2016, 2013; Liteanu and Spiers, 2011; Nakano et al., 2017; Wolterbeek et al., 2016). In cores exposed in batch experiments, the individual dissolution and precipitation reactions are observed in radial zones moving inwards with exposure duration. The inwards progression of these reactions is mostly controlled by diffusion through the sealant microstructure (particularly of CO_2 into the sealant, and of Ca^{2+} outwards from the sealant), and reaction rates, and the extrapolation of attained reaction progress beyond experimental durations may be complicated because of the interplay between these different rates. Furthermore, the rates with which these different reactions progress inwards into exposed samples also depend strongly on the sealant composition (additives added to the OPC, such as fly ash or silica), water-binder ratio, and curing and exposure conditions. In contrast, during forced flow experiments with sufficiently high pressure gradient, the penetration of CO_2 (or CO_2-bearing fluid) into the exposed sample cylinders is controlled by pressure-driven flow, and thus sample permeability.

These experimental findings are supported by an investigation on a cement seal retrieved from a well that was exposed to CO_2 for 30 years (Carey et al., 2007), which shows considerable carbonation along leakage pathways such as the cement-steel and cement-caprock interfaces, but do not show significant degradation of the cement, taken to indicate that the cement was not exposed to a flow of CO_2-saturated water. Likewise, samples of a wellbore seal consisting of Portland-fly ash cement that was exposed to supercritical CO_2 for 30 years in a reservoir containing natural CO_2 showed that exposure lead to varying degrees of carbonation. Here, carbonation was associated with increases in permeability and porosity, and a decrease in mechanical strength. However, despite these negative changes, wellbore seal integrity was maintained (Crow et al., 2009).

Numerical modelling of the impact of CO_2-exposure on cement-based sealants, based on the above observations, has similarly shown that while exposure initially results in the precipitation of $CaCO_3$. Upon continued exposure (in the presence of water), a decrease in pH may cause the $CaCO_3$ precipitated from interactions between cement and CO_2-bearing fluid to dissolve, leaving behind a Ca^{2+}-depleted silica-gel, which is considerably degraded with regards to microstructure (and thus permeability) and mechanical properties (cf. Hernández-Rodríguez et al., 2017). As the penetration depth of CO_2 into well-cured, intact cements may be quite limited, these effects may be of particular importance where leakage-pathways have formed due to other effects, such as thermal cycling, mechanical load changes, or poor bonding at the annular cement-steel interface.

When interpreting the impact of exposure to CO_2 (or other deleterious effects) on sealant integrity through exposure experiments, it is important to distinguish between CO_2-induced microstructural, mineralogical and/or chemical changes that directly and negatively impact sealant quality versus changes that do not directly impact sealant integrity (cf. Zhang and Bachu, 2011). Making this distinction is of key importance for accurately extrapolating the long-term integrity of a sealant. However, the different reactions taking place when a sealant is exposed to CO_2-containing fluids may impact one another. Furthermore, individual reaction fronts may penetrate the sealant matrix at different rates, in particular when their rates are controlled by different kinetic mechanisms (for example, diffusion vs. reaction control). Therefore, a thorough distinction and understanding of these individual processes and their interplay is required. Uncertainties remain whether commonly used wellbore sealants based heavily on OPC will maintain long-term seal integrity under the conditions induced during CO_2-injection and -storage. These uncertainties drive the development of alternative sealants, that either contain OPC as the main binder, or that are based on other cementing technologies. This development of alternative sealants also requires that the key impacts of CO_2-injection and -storage on wellbore seal integrity are identified, and that accurate and reproducible testing methods are established.

The present work was carried out as part of the ACT-funded CEMENTEGRITY project, studying the impact of CO_2-exposure on five different sealant compositions. Three of the sealants were based on Ordinary Portland Cement (OPC), one sealant was based on Calcium-Aluminate Cement (CAC), and one sealant was a one-part geopolymer (GP) in which granite rock waste formed the main precursor. This rock-based geopolymer sealant was developed as an alternative sealant material as part of the CEMENTEGRITY project because geopolymers may offer beneficial properties such as improved resistance to degradation when exposed to CO_2, and because this waste-derived material has a smaller environmental footprint than OPC-based materials (Hajiabadi et al., 2023b). These five sealant compositions were selected to address a range of different sealant types, and to enable a comparison between different mechanisms that could be employed when developing a more CO_2-resistant sealant, such as enhancing a sealant to reduce its permeability (S2), modifying a sealant to harness its carbonation reactions to improve sealant quality (S3), developing a sealant that is less reactive and where carbonation reactions may not impact integrity (S5) or developing a sealant that is non-reactive when exposed to CO_2 (S4). Cured sample cylinders were exposed in batch reactors, to both wet supercritical CO_2, and CO_2-saturated water simultaneously, at simulated downhole conditions (80 °C and 10 MPa), for up to 16 weeks. The impact of high-pressure CO_2 exposure on sealant integrity was subsequently assessed through optical observations, scanning electron microscopy (SEM) with energy dispersive X-ray spectroscopy (EDS) on polished cross-sections, ICP-OES on fluid samples taken from the reactors, and computer tomography (CT) scanning. The combined results of these observations were used to determine the impacts of exposure to CO_2 with particular focus on how these different materials were affected by exposure to CO_2, and on the CO_2-penetration depth. While the present paper only addresses the ability of the five sealants tested to withstand exposure to CO_2-containing fluids and the impact of such fluids on the sealant microstructure and composition, other sealant properties such as mechanical behaviour, permeability, the ability to form a seal, and the ability to withstand changes in temperature; as well as the impact of CO_2-exposure on these properties, are equally important in determining the suitability of a sealant for use in GCS. These properties are addressed by other partners in the CEMENTEGRITY project (cf. Hajiabadi, Khalifeh, and van Noort, 2023; Lende et al., 2024; Li and Pluymakers, 2024a, 2024b; Suryanto et al., 2024).

2. Methods

2.1. Sealant compositions and sample preparation

A summary of the five sealant compositions that were tested is listed in Table 1. Note that all five sealant compositions were formulated to have suitable slurry properties (such as viscosity, density, and setting time) under representative conditions.

The first sealant composition, S1, is a class G (OPC) cement sample,

Table 1
Description of the different sealants.

Sealant	Description	SG
S1	Reference cement, consisting of Class G cement plus 35 % BWOC silica flour.	1.90
S2	Very low permeability composition based on Class G cement plus 35 % BWOC silica flour, adding silica fume and MgO.	1.90
S3	Composition based on S2, replacing 28.5 % of the binder with RePlug™ (olivine-based CO_2-sequestering agent).	1.90
S4	CAC-based sealant composition	1.80
S5	Geopolymer based on powdered granite with GGBFS and micro-silica.	1.90

augmented with 35 % by weight of cement (BWOC) silica flour (mostly to ensure samples would withstand high-temperature curing). This sealant composition was chosen as a reference composition to which the other sealants would be compared, but also to represent cements that might be found in legacy wells in the North Sea and elsewhere. Sealant S2 is a composition based on Class G OPC with silica flour, that has been tailored with silica fume, MgO and other additives to ensure a very low permeability. Sealant S3 is similar to S2 but has been further amended with a high content of ReStone CO_2-sequestering agent, that is mostly based on dunite rock (i.e., olivine – see Kvassnes and Clausen, 2021). The main binder in sealant S4 is a calcium-aluminate cement (CAC). It has further been amended with sources of silica (as discussed in Brothers et al., 2006), $BaSO_4$ to amend slurry density, and selected other additives. Finally, sealant S5 is a one-part ("Just-Add-Water") GeoPolymer (GP) mix that is being developed as part of the Cementegrity project, based on the work reported in (Khalifeh et al., 2016). The precursor material for this GP consists mostly of fine granite powder (5–150 μm) combined with Ground Granulated Blast Furnace Slag (GGBFS) and micro-silica, while the hardener consists of a mix of KOH and K-silicate. A minor quantity of $Al(OH)_3$ is added to adjust the Si/Al ratio of the system (cf. Hajiabadi et al., 2024; Hajiabadi, Khalifeh, van Noort, et al., 2023).

All samples used in this study were prepared by Halliburton in Norway, and were mixed in accordance with API Recommended Practice 10B-2 (API RP 10B-2, 2013). For this study, the slurries were poured into Teflon tubes with an internal diameter of 12 mm, a wall thickness of 5 mm, and a length of approximately 50 cm. The filled tubes were placed in an autoclave filled with regular tap water, and cured for 28 days at 150 °C and 30 MPa. Curing was performed at relatively high temperature in an attempt to ensure our samples were fully cured within 28 days. Once curing was completed, the tubes were retrieved from the autoclave and cut into 30 mm sections. The samples were stored still encased in their tubing and curing water. The weight of the cured samples (without Teflon tubing) was 5.9 – 6.1 g.

Before exposure, the samples were removed from the Teflon tubes by pushing them out carefully with a manually operated hydraulic press. It was found that all samples were covered in a thin outer layer of white precipitate formed between the cured sample and the Teflon tube wall. The thickness of this precipitate layer was dependent on sealant type, with the thickest layers of precipitate observed on S1, while the thinnest precipitate layers were observed on S2. Before exposure tests were started, these precipitate layers were removed from the samples by manual wet-sanding with 1200 grit SiC paper. During the period between sanding and the initiation of experiments (~1–7 days), the samples were stored in their respective brines.

2.2. Exposure under relevant in-situ conditions

An exposure test was started by first measuring the diameter and weight (water-saturated but surface dry) of each sample. The samples were then placed in numbered positions on disk-shaped holders fixed on a threaded stainless-steel rod (see Fig. 1). The lower holder was positioned to be fully submerged in the water phase (bottom) and the upper holder was positioned in the supercritical CO_2 phase (top). While each sample holder had place for five samples, experiments were typically run with 4 samples per holder (as seen in Fig. 1). When the sample holder had been positioned in the autoclave, 200 g of demineralised water was added and the autoclave was closed. Then, the electric heating clamps were mounted around the autoclave and the upper and lower feed tubes were connected. The test system consisted of a setup with five autoclaves that could be operated independently (see Fig. 2). The pressure and temperature of each autoclave was automatically recorded every 5 minutes for the whole experiment.

Each autoclave (holding samples of one specific composition and water) was first deoxygenated by purging low pressure CO_2 (~ 5 barg) for at least 20 minutes. The CO_2 purging was through the bottom tube and out of the top tube, ensuring initial CO_2-saturation and deoxygenation of the water phase. Some water droplets would eventually be splashed to the top set of samples during this process, leaving them partially wetted.

After deoxygenation, the heating was turned on with a target temperature of 80 °C. After 20 – 30 minutes, when the autoclave temperature was close to the target value, high pressure CO_2 was added up to the target pressure. The pressure would subsequently fall as CO_2 was absorbed in the water phase. Additional CO_2 was subsequently added repeatedly until the pressure remained at target (100 ± 2 bar, this was

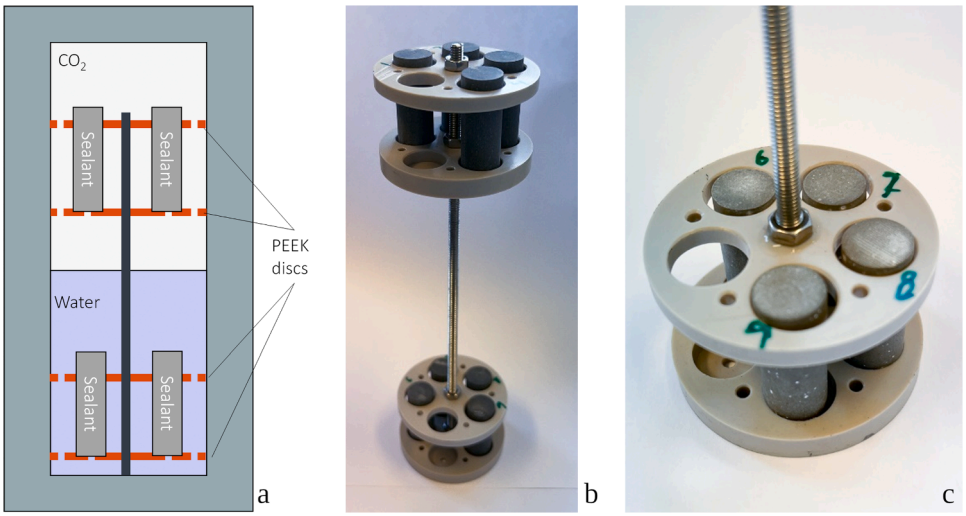

Fig. 1. Sketch of autoclave with sample holder (a), and photos of samples and within a sample holders (b, c).

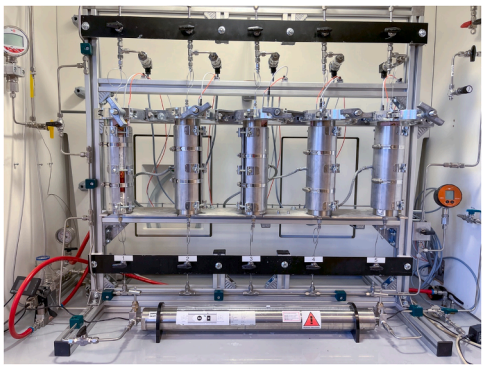

Fig. 2. Picture of the test system with 5 vertical autoclaves and piston cylinder (horizontal) for CO_2 feed.

typically achieved in a few days). Throughout the experiment duration, CO_2 was added as needed to compensate for further absorption and possible small leaks. In general, the cell pressure was maintained between 97–103 bar.

Each experiment was terminated by first turning of the heating (and thus reducing the pressure due to density change). The autoclave was then depressurised in a controlled manner, where CO_2 was taken from the top tube to a heated gas regulator where the pressure was reduced to 1–2 barg. A mass flow controller on the low-pressure side was applied to maintain a slow depressurisation at a fixed bleed-off rate (20 Nml/min for each autoclave). The depressurisation process would typically take 17 – 19 hours. The depressurised autoclave was then opened, and the samples were characterised in the same manner as during start-up (measuring diameter and weight). At this stage, fluid samples were taken for chemical analysis (see Section 2.3.3).

The samples were exposed for up to three subsequent test rounds of 4, 4 and 8 weeks, removing one sample exposed to supercritical CO_2 and one sample exposed to CO_2-saturated water for study and analysis after each round (see Table 2). The autoclave was depressurised between each round of exposure, meaning that the samples had different number of pressurisation-depressurisation cycles depending on the exposure time.

Table 2
Summary of exposure of samples S1 through S4 (top) and S5 (bottom).

Round	Exp. time (weeks)	Accum. exp. time (weeks)	S1-S4 Samples	Test liquid	Liquid sampling
–	-	-	New (unexposed)	Storage liquid	Yes
1	4	4	New (unexposed)	Distilled water	Yes (5 %)
2	4	8	Pre-exposed in round 1	From round 1 + 40 % new distilled water	Yes (5 %)
3	8	16	Pre-exposed in round 1 and round 2	From round 2 + 5 % new distilled water	Yes (5 %)
Round	**Exp. time (weeks)**	**Accum. exp. time (weeks)**	**S5 Samples**	**Test liquid**	**Liquid sampling**
1a	4	4	New (unexposed)	Distilled water	Yes (5 %)
1b	8	8	New (unexposed)	Distilled water	Yes (5 %)
2	8	16	Pre-exposed in round 1b	From round 1b + 5 % new distilled water	Yes (5 %)

2.3. Analyses

2.3.1. Sample preparation

After exposure, the cylindrical sealant samples were cut in half, giving two smaller, equally sized cylinders, using a fine diamond saw. Next, the sawcut surface of one half of each cylinder was ground flat on a diamond grinding disc and the cylinder half was then embedded in Struers EpoFix epoxy resin. Vacuum was applied during embedding to remove air bubbles. Once the resin had hardened, the sample cross-section surface was ground again on the diamond disc, and then ground down to 2500 grit on wet SiC papers. After drying overnight at room temperature, the polished surfaces were vacuum impregnated with low-viscosity Araldite 2020 epoxy resin, the viscosity of which was further reduced by adding a small volume of acetone. Once that resin had hardened, the samples were ground and polished manually, aiming to go just beyond the original sanded surface, and then a final polish was carried out using 3 μm diamond polishing paste on a cloth disc.

2.3.2. SEM with EDS

Cross-sections of exposed and unexposed samples were investigated with SEM and EDS. All samples were carbon coated in the standard manner to prevent charge-buildup. The SEM instrument was operated with 15 kV acceleration voltage. Most pictures were acquired using the backscatter electron detector, configured to maximise atomic number contrast. EDS mapping (chemical composition mapping) was acquired using the AZtec v/6.1 software from Oxford Instruments. Each map was taken over a 800 μm x 550 μm area, with a 1024 × 704 pixels grid, giving a pixel density (resolution) of 0.8 μm x 0.8 μm.

2.3.3. Chemical analysis of reaction fluids

Samples of curing fluid (in which the cured samples were stored, and thus representative of the initial pore fluid within the samples) and fluids retrieved from the autoclaves after exposure were analysed with inductively coupled plasma optical emission spectroscopy (ICP-OES). The fluids retrieved from the reaction vessels were stored cold (~4 °C) until all samples had been collected. Before analyses, the liquid samples were filtered (0.45 μm filters) and diluted with 2 % nitric acid to proper concentrations of targeted elements for ICP-OES. Analyses were then performed using an Agilent 5800 ICP-OES.

2.3.4. CT-scanning and phenolphthalein

CT-scanning was performed on an X-ray micro-tomography (micro-CT) scanner (model CoreTOM, TESCAN), with a spatial resolution (voxel size) of about 13.5 μm. Panthera software (version 1.4, TESCAN) was then used to post-process the images. Scanning was performed on the opposite half-cylinders, cut off when preparing samples for SEM (i.e., the halves that were not impregnated with epoxy). The scans shown below were all taken at 2 mm away from the sawcut surface, to avoid damage induced by cutting. Between exposure and scanning, the samples were stored in small, sealed Ziplock bags. After scanning, the half-cylinders were cut axis-parallel, and phenolphthalein was applied on the sawcut surfaces to visualise carbonation. This was also done on half-cylinder cut-offs of the 4- and 8-week exposed samples.

3. Results

In general, the results showed that the impact of exposure on the sealant samples was strongly dependent on sealant composition and exposure conditions (wet supercritical CO_2 vs. CO_2-saturated water).

3.1. Mass and chemical changes

3.1.1. Sample mass changes

Fig. 3 shows relative average sample mass changes as a function of exposure time. Note that for all samples except S5, at 8 weeks exposure, only the sample that was removed from the vessel for analysis was measured. For samples S1-S3 (all based on OPC), sample masses increased 5–9 % during the first 4 weeks exposure. During the second exposure round (4 + 4 weeks exposure), the changes were relatively small (±1 %), but the mass decreased during the third exposure stage (4 + 4 + 8 weeks). Thus, after 16 weeks exposure, all S1-S3 samples were only up to 6 % heavier than before exposure. Furthermore, the S1 samples exposed to CO_2-saturated water showed the largest relative increases in mass, but also a significantly larger decrease in mass after 16 weeks exposure.

The S4 samples exposed to CO_2-saturated water showed only minor changes in mass (smaller than 1 %). The S4 samples exposed to supercritical CO_2 showed similar relative masses after 8 and 16 weeks exposure as the samples exposed to CO_2-saturated water, but a very strong (almost 10 %) mass decrease after 4 weeks exposure. While a drying out of these samples would best explain this reversible loss of mass, the vessels were cooled before depressurisation and opening, and samples masses were measured quickly upon removal from the apparatus, leaving essentially no time for drying out.

The geopolymer samples (S5) increased 1–2 % in mass during the first 4 weeks exposure, with a larger increase for the sample exposed to wet supercritical CO_2, and subsequently decreased in mass. The S5 samples exposed to CO_2-saturated water had 1–2 % lower mass after 8 and 16 weeks exposure than the starting samples. The S5 samples exposed to wet supercritical CO_2 had 1 % increase in mass after 8 weeks, and a similar mass to starting mass after 16 weeks. Note that the 4-week exposure of S5 was carried out in a previously used vessel, and it cannot be excluded that the measured sample mass changes were impacted by contamination.

3.1.2. Fluid chemical compositions

Fluid samples were taken after each exposure to track changes in fluid chemistry. Key element concentrations in the fluids are given in Fig. 4. In addition, samples of the fluid in which the samples were cured, transported and stored (assumed representative of the pore fluid composition in the samples before exposure) were also analysed, shown as zero exposure time in the graphs. Note that Al-concentrations were below detection limit in all water samples analysed, except for the curing and storage fluids. As the graphs show, most elements reached equilibrium values during the first 4–8 weeks exposure, after which their concentrations in the fluid did not change significantly. Fig. 5 show total cumulative amounts of Si and Ca dissolved from the samples, normalised to the starting mass of the samples present in the water phase during each run. Comparing the graphs presented in Fig. 4, S1 and S2 have considerably higher Ca-contents in the fluids than the other samples. Accordingly, the quantity of Ca dissolved in the second exposure step (from 4 to 8 weeks) from these samples (see Fig. 5b) is considerably higher to compensate for the large fluid samples taken after the 4-week exposure step. However, as the element concentrations are relatively stable after the 4-week exposure step, and precipitation was observed in most cells, the observed quantities of ions in solution are the result of equilibrium between dissolution or leaching from the samples, and precipitation, and accordingly only represent the absolute minimum removed from the samples. Note that as the 4-week exposure of S5 was carried out in a previously used vessel, the fluid composition in this exposure may have been impacted by contamination. This may be particularly apparent in the relatively high Ca-content.

3.1.3. Testing with phenolphthalein

All half-cylinders cut-off when preparing samples for SEM observations were in turn cut in half along their axis. Phenolphthalein was then applied to the sawcut surfaces, to check for pH-decreases indicative of the dissolution (due to carbonation) of $Ca(OH)_2$ (in the OPC-based sealants) or other basic salts (in the GP). This testing showed that already after 4 weeks of exposure, pH-values had dropped to below ~8.5 throughout all samples. Note that, even before exposure to CO_2, the pore fluid in S4 (CAC) does not have a sufficiently high pH for phenolphthalein to be used to detect carbonation effects in this sealant.

3.2. Microstructural development of sealant S1

3.2.1. S1 unexposed reference sample

Freshly removed from their moulds, and with the smooth white outer coating removed, S1 samples are uniform grey. Fig. 6 shows SEM micrographs of a medial cross-section through the unexposed sealant S1, with the thin white precipitate left in place. Micrograph Fig. 6a was taken near the centre of the cylinder, while Fig. 6b shows the sample edge. In these micrographs, silica grains and unreacted clinker particles can readily be identified in the CSH-matrix. Larger, spherical pores (i.e., bubbles) are seen in some images, but not all. Furthermore, the outer precipitate is identified as a ~50 μm thick layer of needle-shaped crystals growing both inwards from the mould surface, and outwards from the sample surface, with open spaces between the two layers. EDS shows these precipitates to consist mostly of Ca-Silicate, most likely CSH-gel, though small loose crystals of $Ca(OH)_2$ were also observed locally

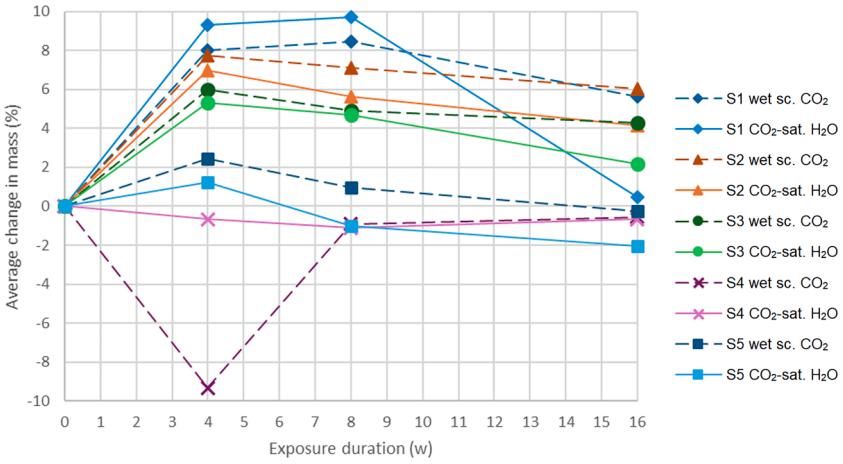

Fig. 3. Average changes in sample mass (mass %) relative to average initial sample mass (before exposure), plotted against exposure time for the five different sealants. Samples were exposed in wet supercritical CO_2 (wet sc. CO_2) and in CO_2-saturated water (CO_2-sat. H_2O).

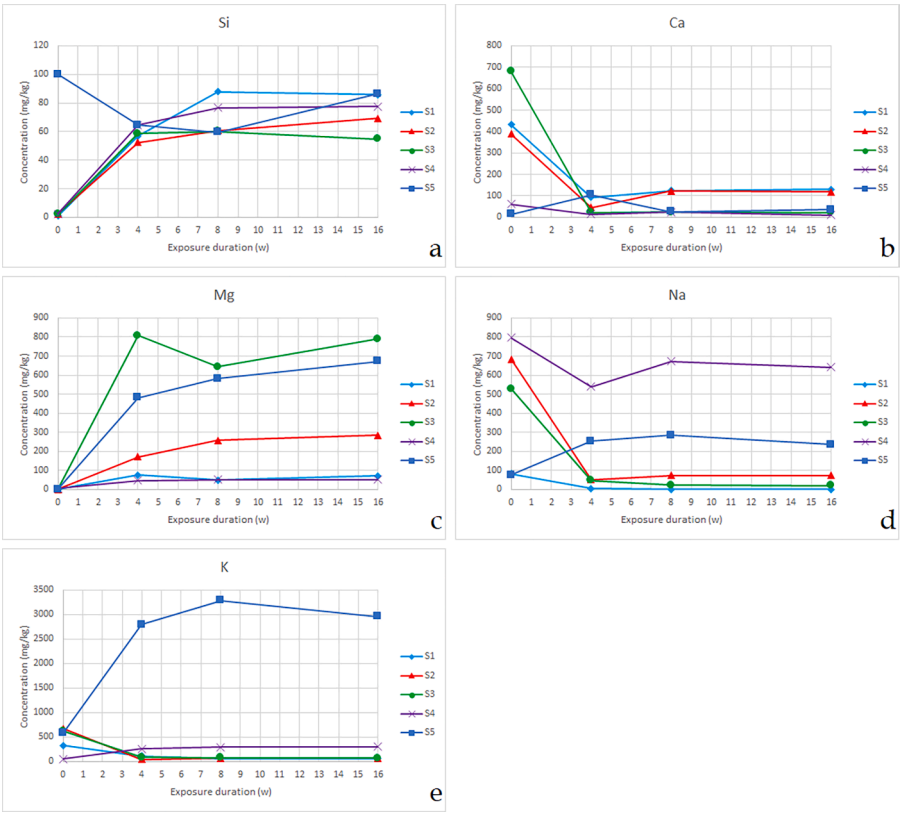

Fig. 4. Element concentrations in sampled fluids, measured using ICP-OES.

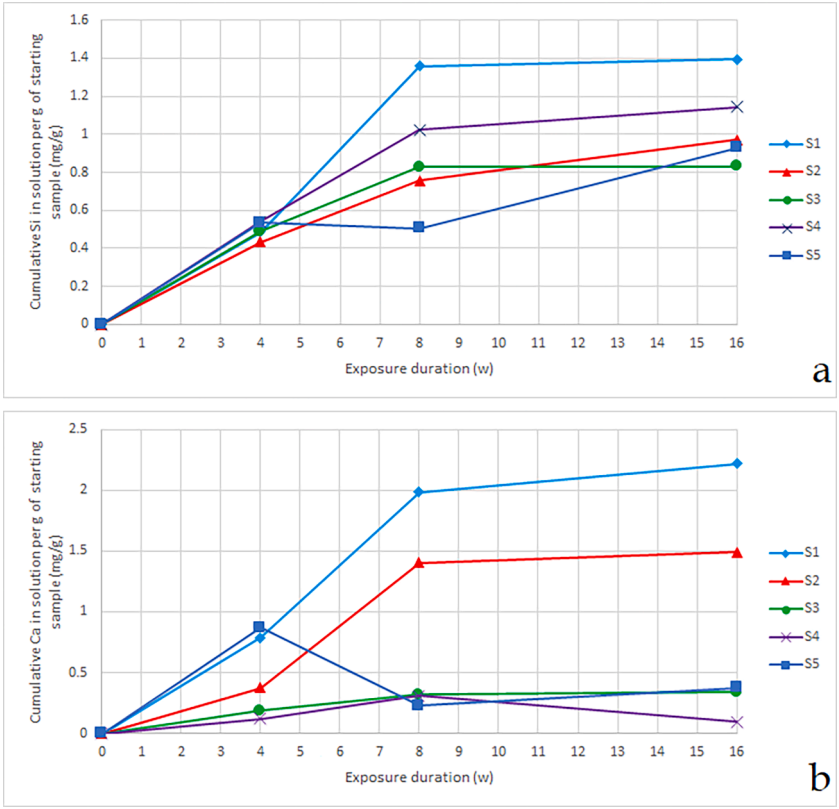

Fig. 5. Cumulative Si (a) and Ca (b) in solution in mg of the element per gram of initial sample mass, corrected for fluid replacement and sample removal.

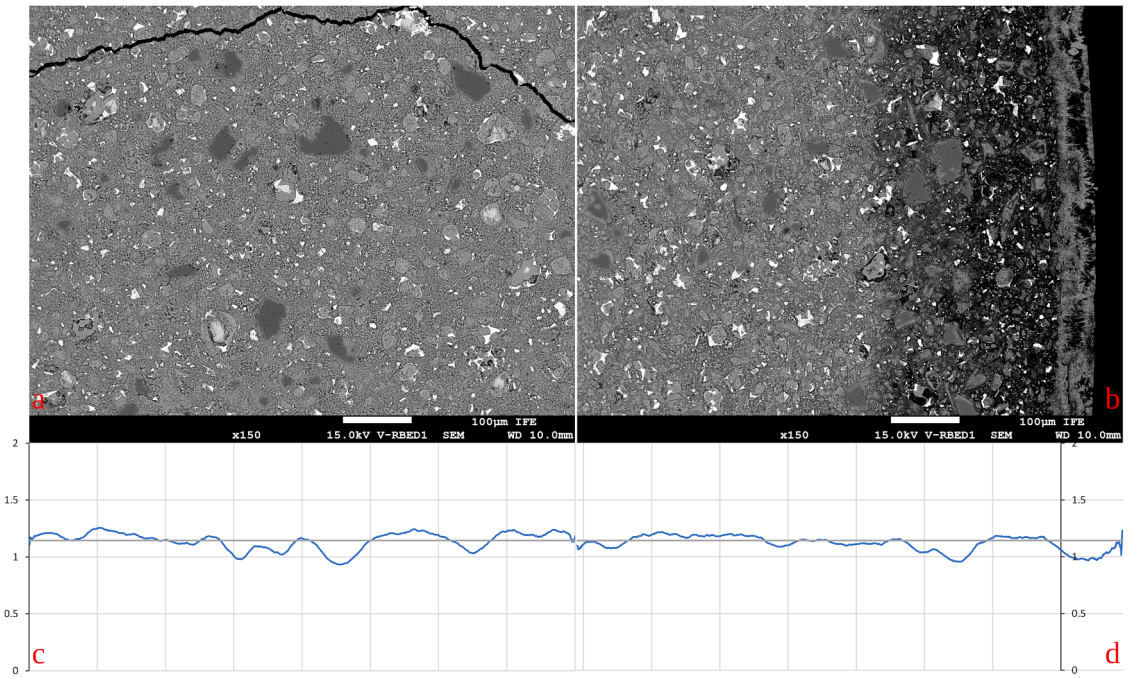

Fig. 6. SEM micrographs imaging a radial cross-section through an unexposed reference sample of S1, showing a) the centre of the sample, and b) the edge of the sample. The Ca/Si-ratio plotted against horizontal location in the micrographs is shown below the micrographs. Full scale on the y-axis is 0–2.

within the precipitate. Furthermore, inwards of the precipitate layer, the outer ~150–250 μm of the sample appears darker, which indicates a lower density due to a higher gel porosity. However, it is important to note that the observed microstructure in the samples studied here is created by grinding and polishing down through an epoxy-filled surface, and may thus also reflect the topology of the surface after initial grinding, before epoxy-impregnation, which is impacted by internal variations in sample hardness (such as contrasts between hard silica-grains and softer CSH-gel, or differences in gel hardness, etc.).

When considering EDS analysis, element ratios can be used to better visualise the variations in chemical composition. Fig. 6c and d show ratios of Ca over Si along horizontal lines across the micrographs shown in Fig. 6a and b. These ratios were calculated for each point along the lines by averaging all Ca-values in one column, and dividing that by the average of all Si-values in the same column. The average Ca/Si-ratio for micrograph Fig. 6a was 1.1, which can be used as a reference value for the overall (starting) sample composition, and is also indicated in the graphs. The Ca/Si ratio plotted from the edge of the sample inwards shows limited variation, which may be attributed to the presence of large silica grains, and also shows that the edge effects observed in Fig. 6b do not reflect a large variation in chemical composition.

Cross-sections from CT-scans of an unexposed reference sample as well as samples exposed for 16 weeks are shown in Fig. 7. A CT-scan through the unexposed S1 reference sample barely shows the very thin outer precipitate layer (and some of the open space within that layer). While a ~240 μm wide ring with slightly reduced density may be observed around the sample edge, potentially corresponding to the darker edge seen in SEM-images, the difference in greyscale, and thus density, seen in the CT-scans is negligible.

3.2.2. *S1 exposed to CO_2-saturated water*

After 4 weeks exposure to CO_2-saturated water, the outer surfaces of S1 samples had changed colour from grey to reddish brown. In addition, white precipitates had started to form on the sample surfaces. After 8 weeks, these precipitates had grown into a near-continuous thin precipitate layer, with locally thicker crusts. After 16 weeks the samples were largely covered in precipitate, and the localised thicker crusts of precipitate had increased in thickness and extent. Fig. 8 shows stitched SEM micrographs from the edge inwards of samples exposed 4, 8 and 16 weeks to CO_2-saturated water, along with their mapped Ca/Si-ratios. Ca-precipitates, most likely carbonates, can be seen on the outer surfaces of the 4- and 16-week exposed samples. Similar precipitates were also present on the 8-week exposed sample, but are not shown in the micrograph presented here. These precipitates correspond to the precipitate layers observed on the samples optically; but some of the precipitates may have been removed during sample preparation for SEM.

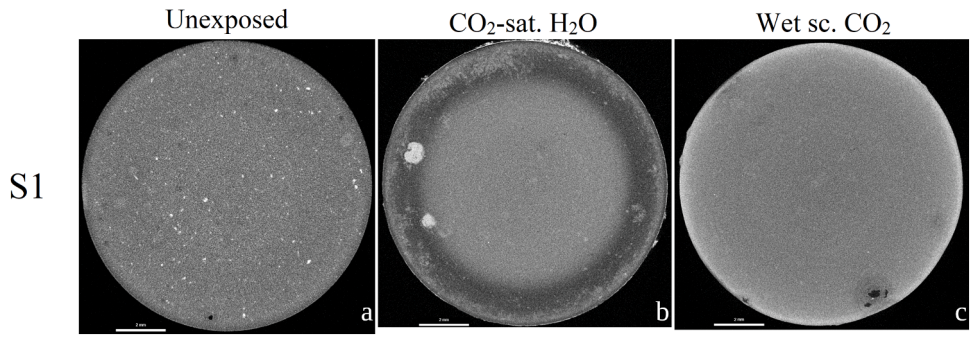

Fig. 7. CT-scans of sealant S1; unexposed, exposed to CO_2-saturated water for 16 weeks, and exposed to wet supercritical CO_2 for 16 weeks.

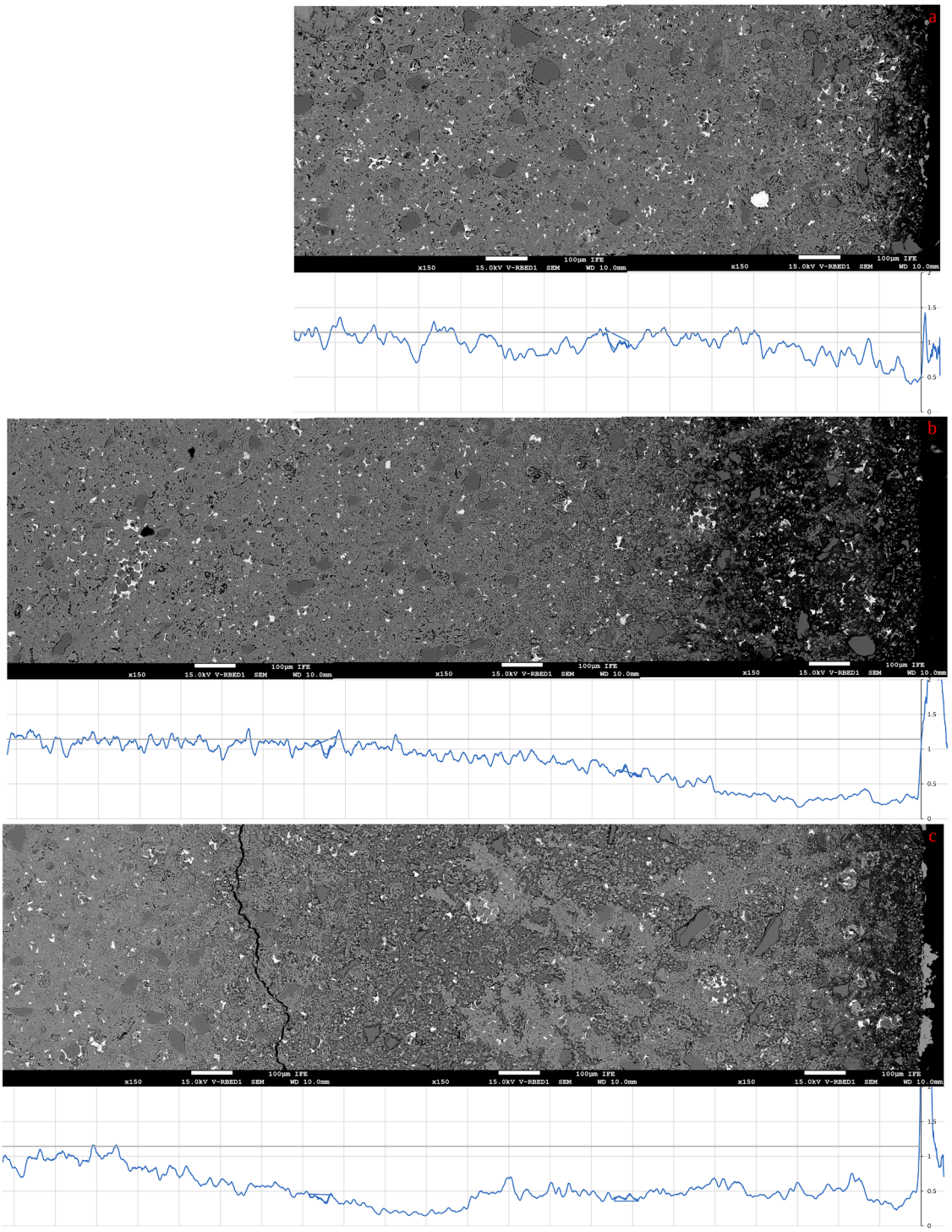

Fig. 8. SEM Micrographs of S1 samples exposed to CO_2-saturated water for 4 (a), 8 (b), and 16 (c) weeks. The graphs underneath each micrograph show the Ca/Si elemental ratios measured along the micrograph using EDS.

Moving inwards from the precipitate, the 4-week exposed sample shows an approximately 130 μm wide zone with a high (apparent) porosity and (likely) low mechanical integrity, indicating that this zone is strongly altered by dissolution and/or leaching. This correlates to a very low Ca/Si-ratio that is depleted down to ~0.4 near the sample edge. Further from the sample edge, the material gradually becomes less altered, while the Ca/Si-ratio also increases gradually. The gel matrix has a more grainy appearance than unaltered matrix material, and gel pores may be filled in by precipitates, likely $CaCO_3$. It should be noted that here, Ca/Si-ratios are still lower than for the unexposed sample. From roughly 400–450 μm from the sample edge, Ca/Si-ratios stabilise around unaltered values, while based on microstructural observations, the matrix still looks somewhat altered by CO_2 down to a depth of ~650 μm. Note that the drop in the Ca/Si-ratio observed at around 800–1000 μm can be ascribed to the two large silica grains in the analysed cross-section.

In the sample exposed for 8 weeks, the depleted outer zone is approximately 900 μm wide. Here, the outermost ~100 μm has a strongly degraded appearance in cross-section, behind which the material integrity starts to improve. Within the outer zone, the Ca/Si-ratio

is strongly reduced to ~0.3, while from ~300 μm it starts to increase gradually. From about 900 to 1150 μm, precipitates fill gel pores and the (apparent) porosity is lower than in the unaltered material. In this zone, the remaining gel is still darker in contrast, indicating Ca-depletion (cf. Kutchko et al., 2008), but gradually becomes lighter and less altered. Likewise, the Ca/Si-ratio increases gradually, until at about 1400 μm from the sample edge, the material appears unaltered.

Finally, the sample exposed for 16 weeks shows a different microstructure. The ~150 μm outer zone has high porosity, suggesting it is mechanically weak, and strongly degraded by leaching or dissolution, in particular in the outermost 50 μm. The Ca/Si-ratio is much lower here, to a minimum value of ~0.2. Moving inwards, a more indurated microstructure is observed, where a precipitate appears to fill the porosity in the sample matrix, resulting in a microstructure with low (apparent) porosity. Here, Ca/Si-ratios range from 0.4 to 0.6. This reaction rim has a very irregular, jagged boundary inwards, and a width varying between 450 and 1000 μm. Inside of this rim, another zone is observed where the microstructure again suggests a softer, more porous material, and where the CSH-gel is relatively dark. At this transition, a second reduction in Ca/Si-ratio to ~0.2 is observed. The Ca/Si-ratio remains relatively constant at this value for about 200 μm, and then gradually starts to increase, which correlates to a gradual strengthening of the gel microstructure, until at ~1900–2000 μm both the microstructure and the Ca/S—ratios no longer show impact by CO_2-exposure.

In a CT-scan of the S1 sample exposed to CO_2-saturated water (see Fig. 7), precipitates on the sample surface can be identified easily, as well as two larger bubbles (partially) filled with precipitate. Considering the penetration of CO_2, and associated reactions with the cement, the scan shows a narrow outer zone with reduced density (~110 μm wide), within which a zone is observed with increased density, which is irregularly delineated, its width varying between ~300–900 μm. Further inwards, densities drop sharply to lower values than at the centre of the sample, and then increase gradually up to constant values, reached at about 2.0 mm from the cylinder edge. These observations agree well with the different microstructural changes observed in the SEM, and indicate that the variations in porosity (or density) apparent in the locally obtained 2D SEM images do indeed reflect 3D porosity changes in the entire sample. Note that, based on testing with phenolphthalein, all $Ca(OH)_2$ in the exposed samples had been dissolved already after 4 weeks of exposure. Ca/Si elemental ratios averaged over maps taken at the centres of the exposed samples were somewhat lower for the samples exposed for 4 and 8 weeks, and slightly elevated for the sample exposed for 16 weeks, but these changes were negligible.

3.2.3. S1 exposed to wet sc. CO_2

Samples of S1 exposed to wet supercritical CO_2 were lighter and somewhat yellowish in colour, with deeper local discolouration to khaki then orange. Local white spots observed at the sample surfaces likely correspond to bubbles in the cement. Thin, very fine deposits can be discerned on the sample surfaces throughout, and on the sample bottom surfaces (where fluid may have been trapped between sample and holder) locally thicker precipitates are found. Fig. 9 shows stitched micrographs of S1 samples exposed directly to a wet supercritical CO_2 phase for 4, 8 and 16 weeks, along with Ca/Si-ratios mapped along these images. The sample exposed for 4 weeks shows a very thin (few μm at most) outer layer of precipitate, and then a softened zone, roughly ~150 μm wide, with high (apparent) porosity, and depleted Ca/Si-ratios, especially in the outer ~60 μm. Within that, a somewhat densified, carbonation zone is observed down to 340 μm into the sample, followed by a zone of minor Ca/Si-depletion. These changes (in particular the leached outer zone) are not observed consistently around the sample, since at other locations around the edge, only minor densification (porosity-filling) of the gel microstructure is observed in the outer ~100–160 μm, along with somewhat elevated Ca/Si-ratios. From 420 μm from the edge onwards, the Ca/Si-ratios and microstructural observations indicate that the sample is relatively unaltered, though testing with phenolphthalein has shown the full sample to be depleted in $Ca(OH)_2$. However, note that the Ca/Si-ratios on the centre maps of the exposed samples, changes in chemical composition were relatively minor.

The 8-week exposed sample (Fig. 9b) also shows a strongly affected outer zone, with reduced structural integrity and increased porosity in the outer ~150 μm of the sample; most notably in the outer ~40 μm. Further inwards, to about 320 μm from the sample edge, the porosity of the material decreases, first due to precipitation of larger grains or agglomerates of calcite within the open pores, and, where the cement gel matrix was maintained, within the pores in this matrix. This precipitation results in a relatively coarse microstructure, and is correlated to a sharply increasing Ca/Si-ratio, resulting in relatively high Ca/Si-ratios between ~150 to 300 μm from the edge. Further inwards, between ~320–540 μm, the cement gel matrix looks darker, i.e., affected by Ca-leaching, even though Ca/Si-ratios do not deviate significantly from average unaltered gel. Based on the Ca/Si-ratio and the microstructural observations reported here, the sample microstructure appears unatered from about 540 μm inwards.

In the sample exposed to wet supercritical CO_2 for 16 weeks, precipitation in the gel matrix (again distributed heterogeneously) lead to a denser microstructure with reduced porosity in the outer ~500 μm of the sample, though the changes are most apparent in the outer ~250 μm where the gel structure also appears relatively coarse. This correlates well with a strongly increased Ca/Si ratio that decreases sharply from the edge, down to a constant value of roughly 1.6 between 10 and 90 μm from the edge, and then decreasing down to normal values at ~420 μm (if values strongly affected by large SiO_2 grains are disregarded).

The CT-scanned cross-section of this same sample (see Fig. 7) shows an outer zone with elevated density followed by a gradual transition moving inwards. This outer zone, from the edge of the sample to where the density starts to decrease, has a width of roughly 240 μm, while a maximum bound for this zone to where the density becomes stable (and thus the same as at the centre of the sample) suggests a total width of about 470 μm.

3.3. Microstructural alteration of sealant S2

3.3.1. S2 unexposed reference sample

When removed from the moulds, samples of S2 have only a thin, translucent coating of white precipitate. Removal of this outer layer results in a homogeneously dark grey sample. Fig. 10 shows SEM micrographs of a polished cross-section through sample S2 with the outer precipitate left in place. At the sample edge, a thin dark outer layer is observed, roughly 10–30 μm thick, with a very fine needle-like precipitate on the outer edge. Locally, a similar opposite layer is observed, suggesting that the precipitate may have been a similar double layer as that observed on S1, but that the outer layer was mostly lost during removal of the sample from the mould. In addition, the images show that S2 has a denser microstructure than S1, with a higher content In granular materials with grain sizes below ~100 μm.

As in S1, phases such as unreacted clinker minerals (typically observed as large grains consisting of multiple phases in a matrix with high density), quartz or silica (angular, evenly dark grey grains), and Mg $(OH)_2$ (typically showing as dark, porous areas within the gel matrix) are readily identified in EDS maps. Ca/Si-ratios based on the obtained EDS maps are plotted in Fig. 10c and d. The average Ca/Si-ratio for the SEM micrograph shown in Fig. 10a (taken near the centre of the reference sample) is 0.94.

CT scans of the unexposed reference sample of S2 (see Fig. 11) show a homogeneous sample density, with some white spots indicating grains of higher density; most likely unreacted clinker.

3.3.2. S2 exposed to CO_2-saturated water

After the 4 and 8 week exposures to CO_2-saturated water, samples of S2 were somewhat discoloured to a brownish grey. Samples exposed for

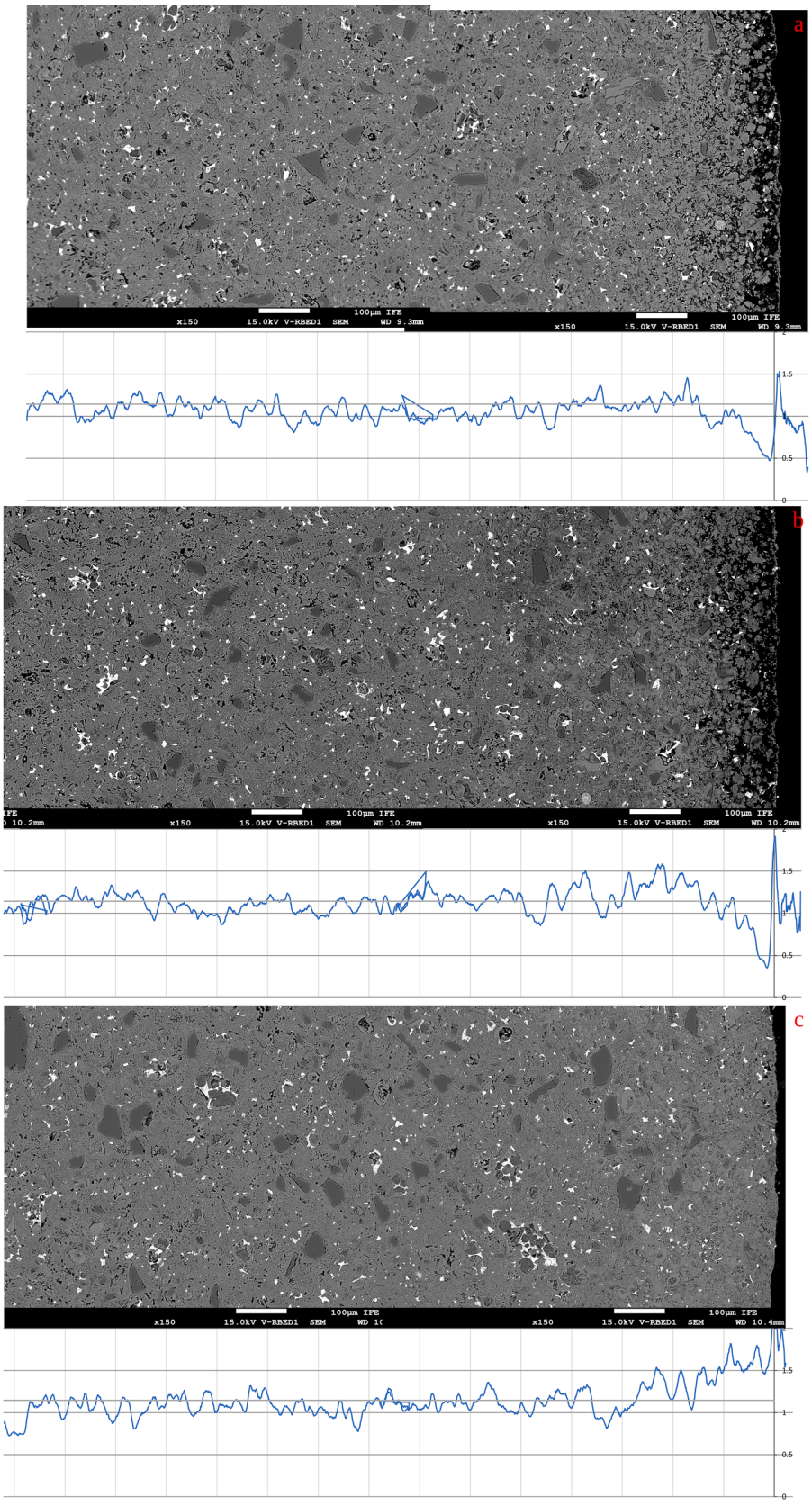

Fig. 9. SEM Micrographs of S1 samples exposed to wet supercritical CO_2 for 4 (a), 8 (b), and 16 (c) weeks. The graphs underneath each micrograph show the Ca/Si elemental ratios measured along the micrograph using EDS.

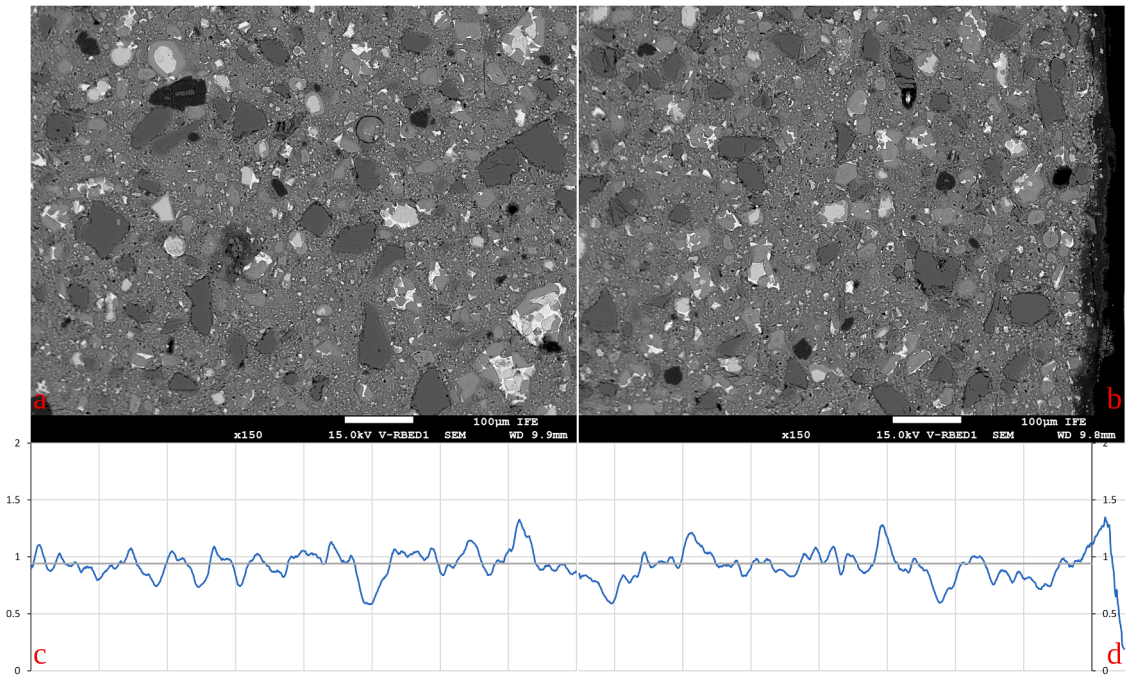

Fig. 10. SEM micrographs imaging a radial cross-section through an unexposed reference sample of S2, showing a) the centre of the sample, and b) the edge of the sample. The Ca/Si-ratio plotted against horizontal location in the micrographs is shown below the micrographs.

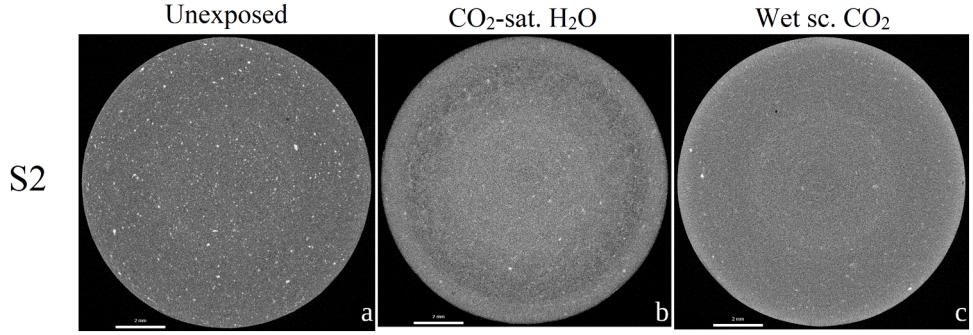

Fig. 11. CT-scans of sealant S2; unexposed, exposed to CO_2-saturated water for 16 weeks, and exposed to wet supercritical CO_2 for 16 weeks.

16 weeks appeared lighter, due to a thin layer of light-coloured precipitate, and were discoloured further to somewhat greenish yellow tints. Fig. 12 shows SEM micrographs of S2 samples exposed to CO_2-saturated water, along with mapped Ca/Si-ratios. In all samples, exposure lead to a narrow outer zone that was strongly altered due to exposure to CO_2-saturated water, where Ca/Si-ratios are depleted leaving behind a matrix porous looking material that appears to have limited structural integrity. The width of this zone was about 20–40 µm wide for all these samples.

In the sample exposed for 4 weeks, this highly altered zone transitions sharply into a zone where the gel matrix has a relatively fine, grainy appearance and reduced porosity, suggesting densification due to carbonate-precipitation. This transition is correlated to a sharp increase in the Ca/Si-ratio. Moving inwards, the microstructure gradually coarsens and becomes more porous, as it transitions into a similar microstructure as that observed in the centre of the sample. At the same time, the Ca/Si-ratio gradually increases. Based on both microstructure and Ca/Si-ratio, the impact of exposure to CO_2-saturated water reached about 400 µm into the sample.

In the 8- and 16-week exposed samples, the outer, strongly altered zone transitions into a secondary altered zone, where the gel matrix is darker, but gradually becomes lighter and more intact. For the 8-week exposed sample, this reaches to a depth of about 100 µm from the sample edge, though the transition is relatively irregular. The heavily depleted Ca/Si-ratio shows a steep increase up to this depth. Further inward, a third zone is observed with a similar denser, finer microstructure as described above, though the distribution of this densification is somewhat more uneven. The Ca/Si-ratio increases more gradually, and then stabilises at a somewhat depleted value compared to the unexposed reference sample. From about 460 µm, the matrix porosity is higher again, and the microstructure starts to coarsen. While at this depth the Ca/Si-ratio drops sharply, and then increases again, this dip is caused by the alignment of a number of quartz grains seen in the micrograph. From a depth of about 820 µm, the sample microstructure appears relatively unaffected by exposure, though the Ca/Si-ratios are still somewhat depleted compared to the unexposed reference sample, and testing with phenolphthalein has shown that all $Ca(OH)_2$ has been dissolved.

In the sample exposed for 16 weeks, a fine granular microstructure with reduced porosity is seen from about 100 down to a depth of 580 µm, though most notably so between 100 and 300 µm from the edge. Ca/Si-ratios increase from the edge inwards to ~500 µm, where the ratio appears to stabilise at somewhat depleted values. While this increase is quite steep in the outer 100 µm, it becomes more gradual between 100

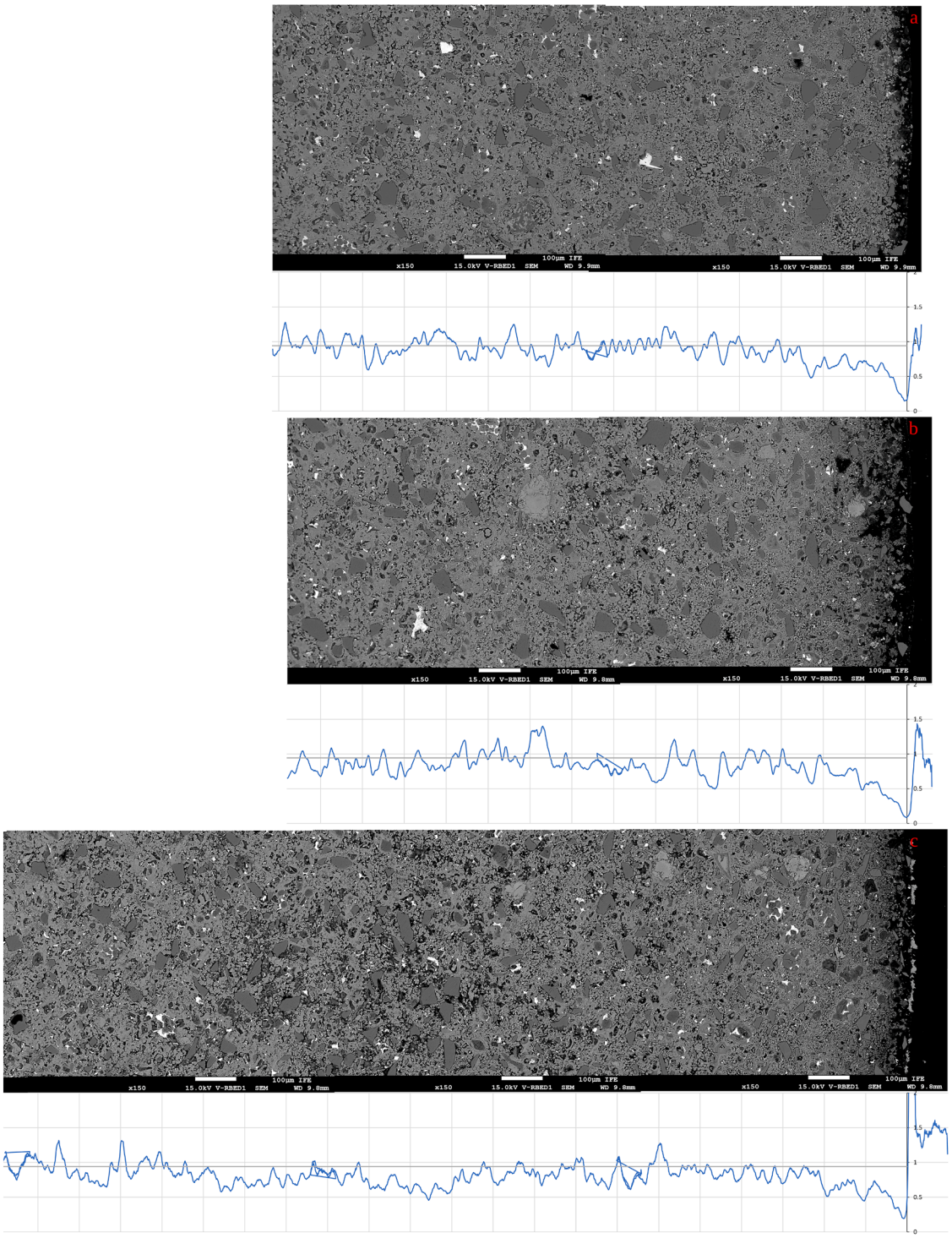

Fig. 12. SEM Micrographs of S2 samples exposed to CO_2-saturated water for 4 (a), 8 (b), and 16 (c) weeks. The graphs underneath each micrograph show the Ca/Si elemental ratios measured along the micrograph using EDS.

and 300 μm, and even slower from 300 μm inwards. From ~800 to 1400 μm from the sample edge, larger pores start appearing in the micrographs, and the microstructure transitions to a coarser structure with higher porosity. This is associated with a minor depletion of the Ca/Si-ratio down to about 1800 μm from the sample edge.

A CT-scan of the S2 sample exposed to CO_2-saturated water for 16 weeks (see Fig. 11) mostly shows a very thin outer edge with reduced density, about 50–60 μm wide (i.e., only about 5 pixels wide). Within that, a roughly 800 μm wide zone is observed, showing a minor increase in density (i.e., a reduction in gel porosity). Finally, inwards of this zone with elevated density, a ~1020 μm wide zone with reduced density is observed, giving a total alteration depth of about 1880 μm. Based on testing with phenolphthalein, all $Ca(OH)_2$ had been dissolved from all exposed samples. This was associated with a small decrease in Ca/Si-ratios at the centres of all exposed samples.

3.3.3. *S2 exposed to wet supercritical CO_2*

S2 samples exposed to wet supercritical CO_2 show minor greenish

brown discolouration, mostly around the bottoms and tops of sample cylinders, where some liquid water may have been trapped between the sample surface and the sample holder. Significant surface precipitation was not observed. SEM micrographs of S2 samples exposed to wet supercritical CO_2 are shown in Fig. 13. Micrographs for all three exposure durations show an outer zone with some relatively coarse pores, and a width of about 90–120 μm, that does not clearly depend on exposure duration. Note that the large pores seen here are very localised, and do not appear interconnected. Inwards from this zone, all three samples show a zone with reduced porosity and a relatively fine, granular matrix microstructure.

Comparing the three samples, the degree to which porosity appears reduced, and the width of these zones both appear to increase with increasing exposure duration. For the 4-week exposed sample, the fine-granular microstructure transitions into an unaltered microstructure about 540 and 800 μm from the sample edge. Within this zone, porosity reductions are relatively minor, and mostly confined to the outer 300 μm, as well as some localised areas of limited extent. The Ca/Si-ratios may be somewhat depleted near the outer part of this sample, but do not show strong variations across these zones.

For the 8-week exposed sample, a more pronounced decrease in porosity is observed to about 400 μm from the sample edge. From 400 to 920 μm inwards, the microstructure increases in porosity, and becomes less fine-grained. In the outer edge of the sample, Ca/Si-ratios are depleted and increase rapidly. Between 70 and 340 μm from the sample edge, Ca/Si-ratios are slightly elevated over the reference value.

For the 16-week exposed sample, the outer zone where cement is degraded is ~120 μm wide, and thus somewhat wider than for the other samples, and it is associated with a somewhat reduced Ca/Si-ratio. This zone then transitions sharply into a zone where porosity is reduced strongly, and where Ca/Si-ratios increase sharply. Very low porosities are maintained to a depth of about 340 μm, from where porosity starts to increase gradually. Here, the microstructure is of the matrix is relatively fine-grained, but also coarsens gradually. At about 1020 μm from the sample edge, the microstructure appears unaltered. Between 100–460 μm from the sample edge the Ca/Si-ratio is somewhat elevated .

The CT-scan of the 16-week exposed sample (see Fig. 11) shows a minor increase in density that is not sharply delineated from the edge, and reaches up to about 680 μm into the sample. However, based on testing with phenolphthalein, all $Ca(OH)_2$ had been dissolved from the exposed samples even after only 4-week exposure, leading to a decrease in Ca/Si-ratios at the centres of all samples.

3.4. Microstructural alteration of sealant S3

3.4.1. S3 unexposed reference sample

When removed from the moulds, samples of S3 have somewhat grainy and uneven coating of white precipitate. Removal of this outer layer results in a homogeneously dark grey sample, similar in colour to S2. Fig. 14 shows SEM micrographs of the centre and the edge of a polished cross-section through sample S3 with the precipitate left in place. Images show large grains of olivine and other minerals found in the dunite used, as well as SiO_2 and some unreacted clinker surrounded by a relatively soft gel matrix. In Fig. 14b, showing the edge of the sample, the precipitate is seen as a thin, <10 μm thick layer of needle-shaped crystals growing outward from the sample surface, composed of Ca-silicate. Note that this precipitate is variable in thickness around the sample, from a few up to several 10′s of μm. The average Ca/Si and Mg/Ca elemental ratios for the unexposed reference sample centre map shown in Fig. 14a are 0.87 and 0.31, respectively.

S3 contains a large fraction of larger mineral grains (mostly silica/quartz, and olivine with associated minerals) that are relatively hard, while the cement-gel matrix around these grains appears relatively soft. As a result, the initial grinding created a surface with height differences between grains and gels. Therefore, the final surface obtained after subsequent resin-impregnation, re-grinding, and polishing was likely impacted by these processes to a larger extent than the other samples. This should be taken into account when assessing the S3 microstructures, especially with regards to apparent porosities; such apparent porosities may represent an interplay of actual porosity, and hardness contrasts.

The CT scan of the unexposed sample (see Fig. 15) shows a mostly uniform microstructure, in which larger grains (likely mostly olivine) are easily recognised. The outer rim of the sample, about 80–90 mu wide, shows a minor increase in density.

3.4.2. S3 exposed to CO_2-saturated water

Samples of S3 exposed to CO_2-saturated water acquired a powdery green surface layer, that is rubbed off easily. The SEM micrographs in Fig. 16 shows cross-sections of samples exposed to CO_2-saturated water. As the images show, exposure mostly lead to changes in the gel matrix, defined by (at least) three different microstructures that progressively move inwards into the samples. The outermost zone presents a leached microstructure, recognizable in the images as finer gel particles among the larger silicate grains, and a higher apparent porosity. In the samples exposed for 4, 8 and 16 weeks, the width of this zone ranges from 100 to 190 to 400 μm, respectively. This outer zone is associated with a depleted Ca/Si-ratio, especially in the outer 30 to 50 μm, resulting in a high Mg/Ca-ratio in the same zone. Here it should be noted that the Mg-contents in the outer parts of the 4-wk and 8-wk samples shown are also impacted by large Mg-silicate grains within the area analysed.

Moving inwards, this zone transitions into a second reaction zone, where the matrix has a somewhat coarser granular structure, though still relatively fine, and where porosity appears reduced. Here, the matrix granulates are typically seen to have darker centres surrounded by lighter rims. In the 4-week exposed sample, the Ca/Si-ratio increased gradually from the edge inwards, and in this zone reaches slightly elevated values compared to the reference sample, before dropping quite sharply at about 450 μm. From here, the resulting gel microstructure becomes more porous and less fine, while Ca/Si-ratios stabilise around reference values. Interestingly, Mg/Ca-ratios are slightly depleted from about 190 to 550 μm into the sample; i.e., somewhat shifted from where Ca/Si-ratios are elevated. Then, from ~1280 μm from the edge, the sample microstructure looks similar to that observed at the core of the sample. However, the island-like matrix microstructure observed here was not observed in the starting material, indicating microstructural change due to carbonation (as confirmed using phenolphthalein). It should be noted that the depth to which these microstructural variations penetrated into the 4-week exposed samples may be somewhat variable, as at other locations around the same sample, microstructures that looked similar to those observed at the core were found at only 240 μm from the sample edge.

In the cross-section through the 8-week exposed sample shown here, the second zone (recognised by the darker-cored, finer gel particles) transitions into a microstructure comparable to that observed at the centre of the sample between ~450 and 600 μm from the edge. Here, Ca/Si-ratios are somewhat depleted and increase very gradually down to 830 μm from the edge, but are also somewhat depleted deeper into the sample. However, it should be noted that the ratios measured here are impacted by the presence of some very large (>300 μm) olivine grains in this cross-section.

In the sample exposed for 16 weeks, the second reaction zone penetrates to about 1400 μm from the sample edge. Within this zone, the gel microstructure gradually coarsens, while the apparent porosity is variable. The Ca/Si-ratio increases very gradually throughout this zone, and then stabilises at below-reference values at about 1000 to 1100 μm.

Zooming in on the second reaction zone in the S3-samples, the lighter rims around the darker particles observed in the sample matrix are identified as precipitates with needle-like growths penetrating into the open pore space around these particles.

The CT-scan on this sample (see Fig. 15) shows strong, but localised density loss (i.e., dissolution or leaching) within the outer ~190 μm of

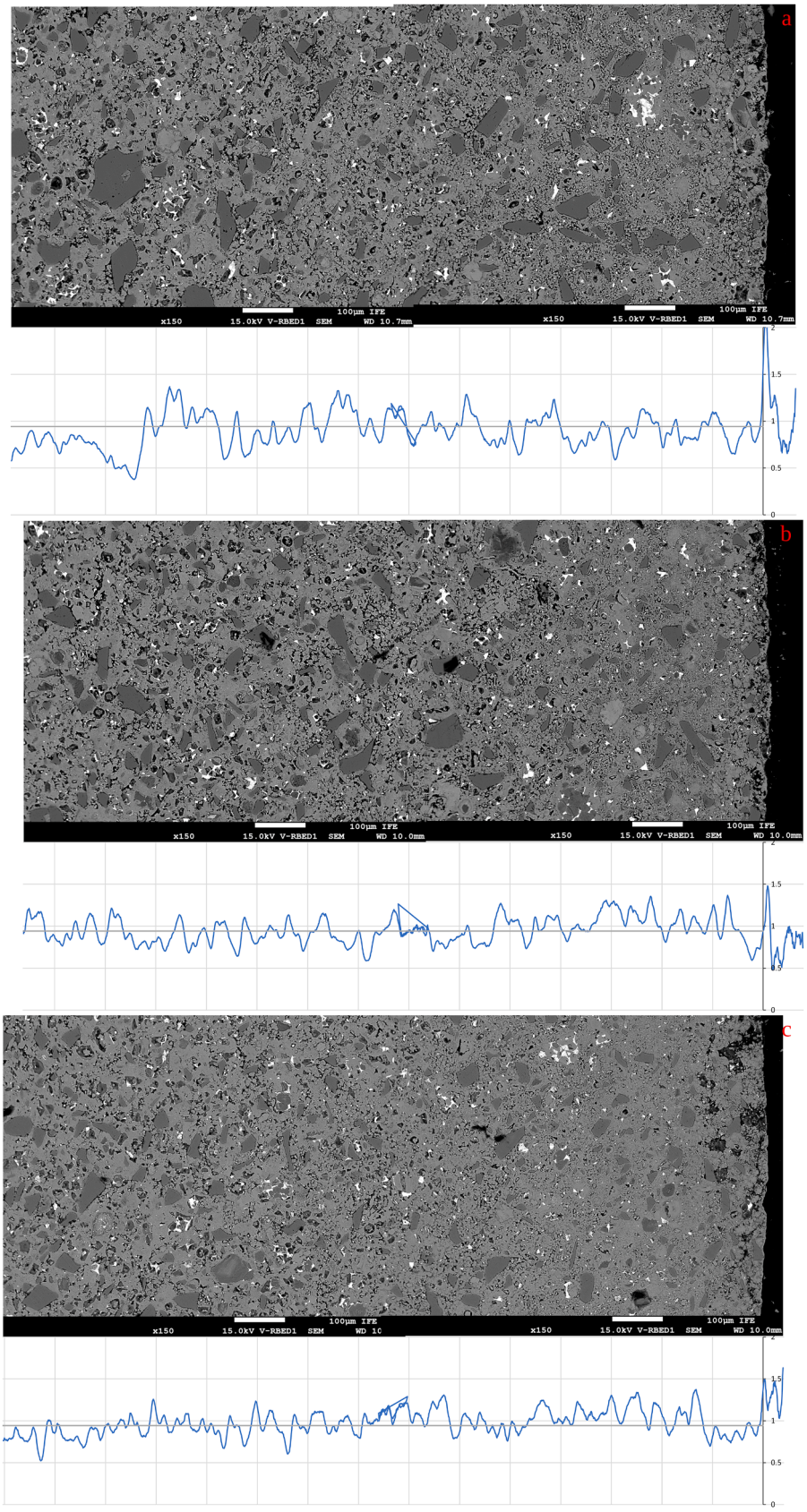

Fig. 13. SEM Micrographs of S2 samples exposed to wet supercritical CO_2 for 4 (a), 8 (b), and 16 (c) weeks. The graphs underneath each micrograph show the Ca/Si elemental ratios measured along the micrograph using EDS.

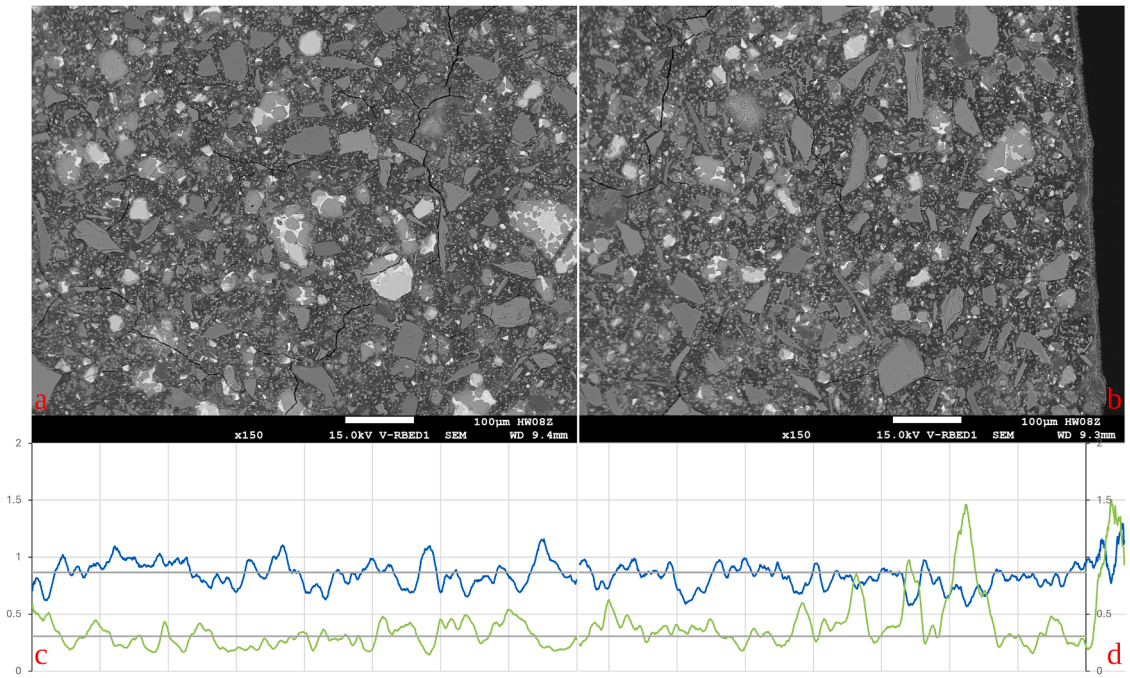

Fig. 14. SEM micrographs imaging a radial cross-section through an unexposed reference sample of S3, showing a) the centre of the sample, and b) the edge of the sample. Shown below the micrographs are the Ca/Si (blue) and Mg/Ca (green) elemental ratios plotted against horizontal location in each micrograph.

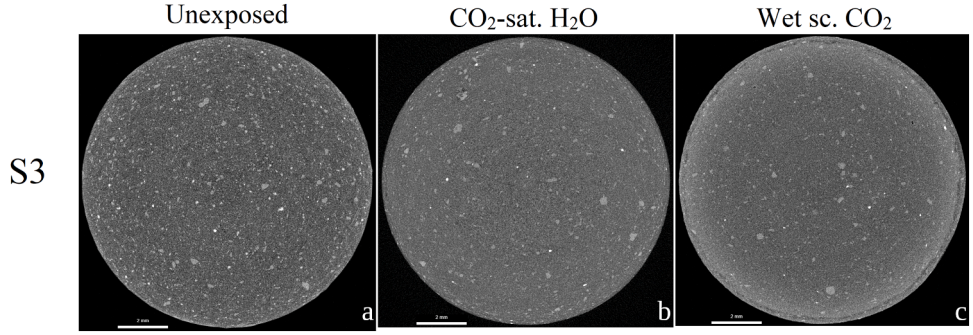

Fig. 15. CT-scans of sealant S3; unexposed, exposed to CO_2-saturated water for 16 weeks, and exposed to wet supercritical CO_2 for 16 weeks.

the sample. Furthermore, in the outer ~500 µm the microstructure appears finer than inwards. From about 1550 to 1910 µm from the edge, the sample has a somewhat lower density, with coarser porosity, than the outer part, suggesting some densification (carbonation) of the sample took place down to about this depth. Full dissolution of $Ca(OH)_2$ from the exposed samples (as determined using phenolphthalein) is associated with a distinct drop in Ca/Si-ratios even at the centres of these samples.

3.4.3. *S3 exposed to wet supercritical CO_2*

Samples of S3 exposed to wet supercritical CO_2 showed minor brownish-green surface discolouration, mostly at the ends where water might have been trapped between sample and holder. Otherwise, optically, these samples did not show discernible external change. Considering the SEM micrographs, presented in Fig. 17, there is an extremely thin outer precipitate on all three samples (few µm in thickness at most). Within that, a fine granular matrix is observed. In the sample exposed for 4 weeks (as shown here), the (apparent) porosity of this matrix decreases fairly sharply from about 50–60 µm from the sample edge. At that same point, the depleted Ca/Si-ratio starts to increase, and there is a peak in the Mg/Ca-ratio. From about 120 µm, the Ca/Si-ratio in this sample stabilises around the reference value. However, the fine-grained microstructure is maintained down to about 630 µm from the edge, and then transitions gradually into coarser island-like matrix microstructure at ~850 µm.

In the 8-week exposed sample, a similar, finer-grained outer zone is observed, transitioning to the coarser microstructure at ~590–780 µm. While the entire outer zone looks relatively porous, this may be in part due to sample impregnation and polishing effects as noted above. Within the finer-grained outer rim, the outermost 130 µm has higher porosity. Here, the Ca/Si-ratio is quite depleted. Between 130 and 310 µm, the (apparent) matrix porosity decreases gradually, while the Ca/Si-ratio increases to the unaltered average. The Mg/Ca-ratio in the outer zone is quite elevated, with a peak at about 90 µm, followed by a sharp drop between 90 and 140 µm. However, the Mg/Ca-ratios observed here are impacted by the presence of Mg-silicate grains in a relatively open matrix.

The outer 200 µm of the sample exposed for 16 weeks has a fine-grained matrix, with relatively high (apparent) porosity, and depleted Ca/Si-ratio. From about 200 to 300 µm, the Ca/Si-ratio increases to approximately the reference value, and then decreases very gradually to somewhat below reference, stabilizing from about 540 µm. The increasing Ca/Si-ratio is associated with a decreasing matrix porosity, and then, from about 300 µm, a coarsening of the matrix microstructure.

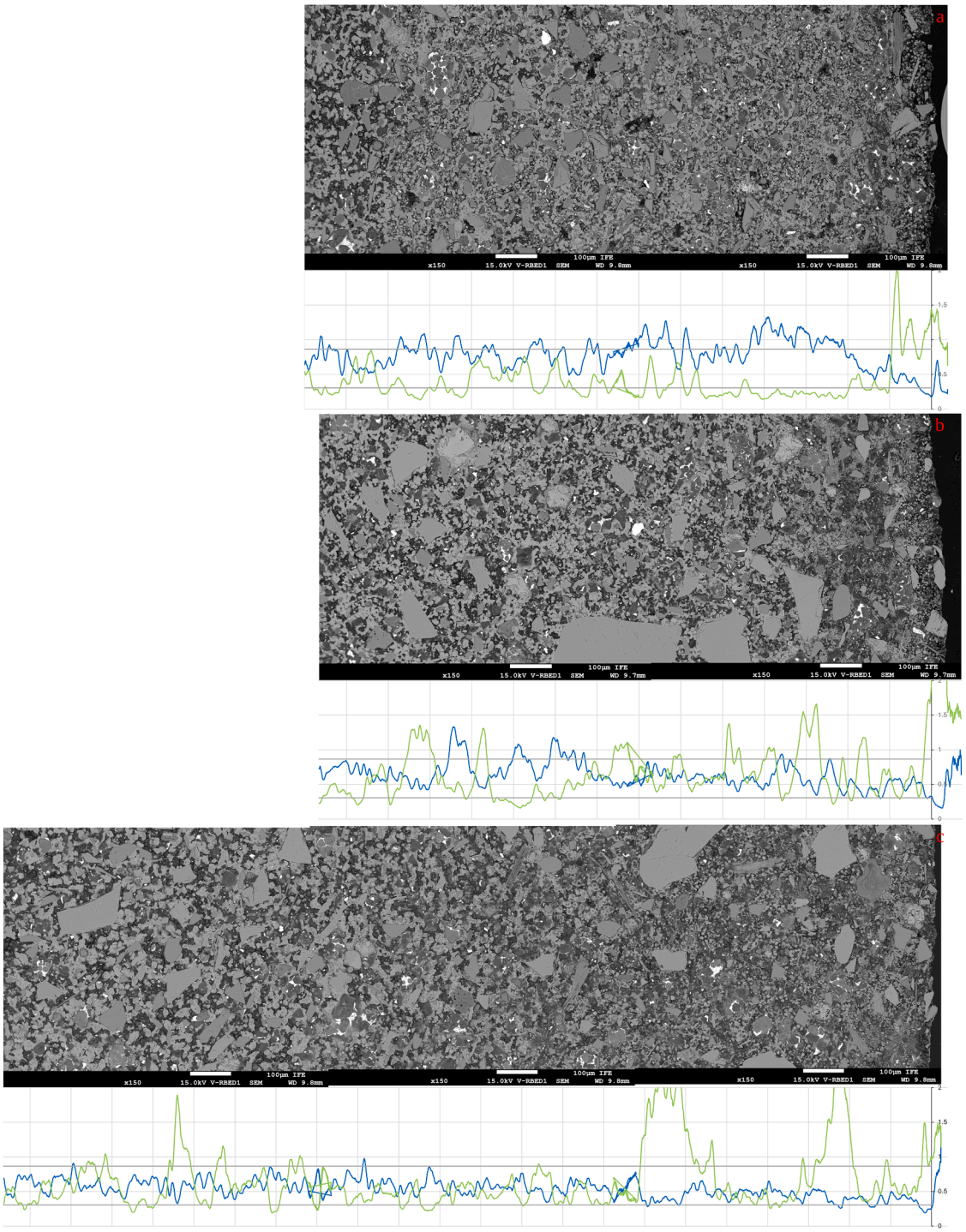

Fig. 16. SEM Micrographs of S3 samples exposed to CO_2-saturated water for 4 (a), 8 (b), and 16 (c) weeks. The graphs underneath each micrograph show the Ca/Si (blue) and Mg/Ca (green) elemental ratios measured along the micrographs using EDS.

From about 1100 to 1320 μm, the matrix porosity increases, and the microstructure becomes similar to that found at the centre of the sample. Interestingly, the Ca/Mg-ratio peaks at about 200 μm from the sample edge, and then drops sharply. While this coincides with the changes in Ca/Si-ratio and gel microstructure, it is also again associated with an alignment of Mg-silicate grains at this distance from the sample edge.

The CT-scan of this sample (see Fig. 15) shows localised signs of degradation (i.e., local decreases in density) as well as some enhanced density areas in the outer ~250 μm, followed by densification (interpreted as carbonation) down to about 1100 μm from the edge, fading out gradually towards the sample core. Testing with phenolphthalein shows that all exposed samples are fully depleted in $Ca(OH)_2$, leading to a drop in Ca/Si ratios at the centres of these samples.

3.5. Microstructural alteration of sealant S4

3.5.1. S4 unexposed reference sample

Upon removal from the moulds, S4 samples are covered with a relatively thick coating of white precipitate, that is relatively uneven and rough. In SEM micrographs (Fig. 18), the coating is seen as a double

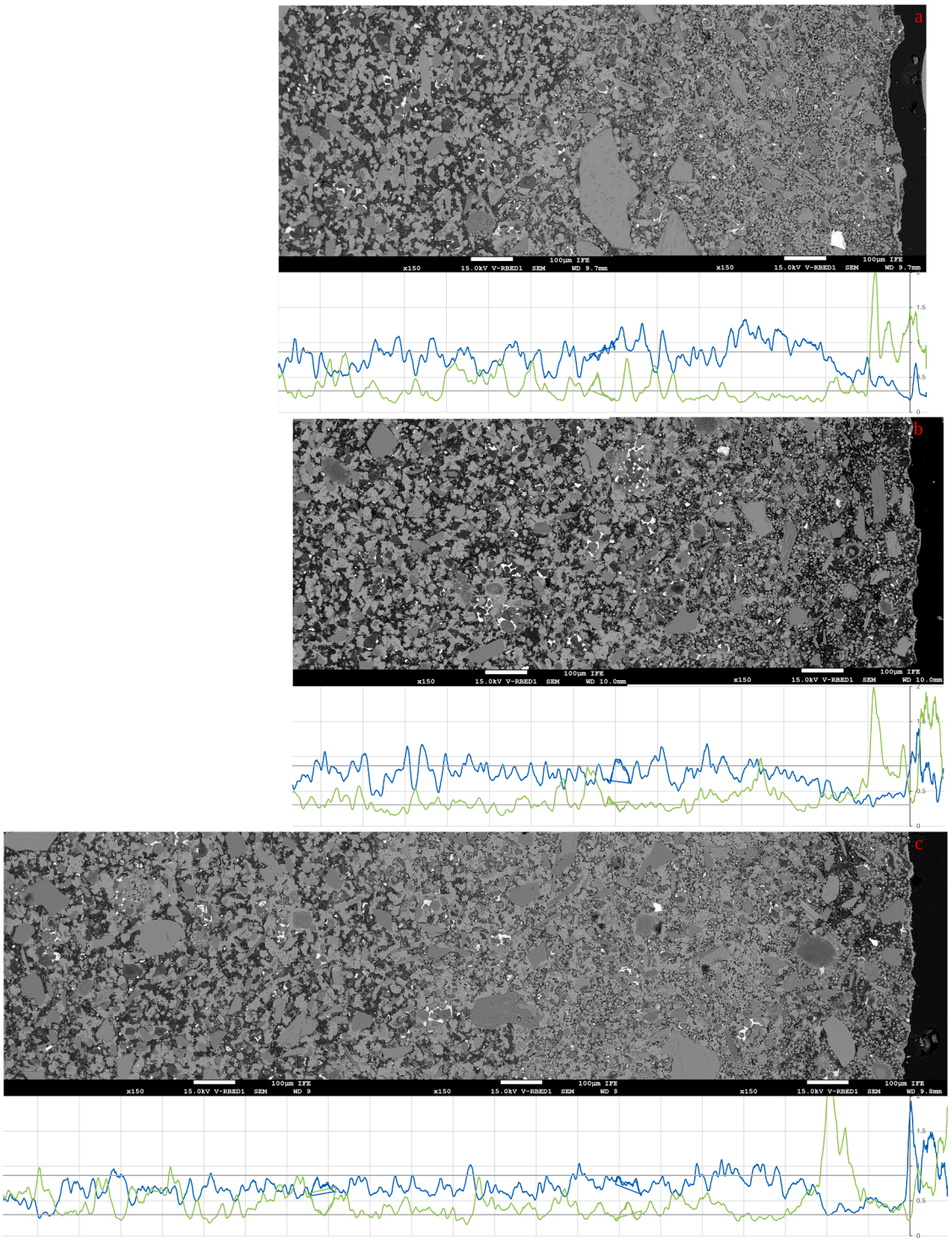

Fig. 17. SEM Micrographs of S3 samples exposed to wet supercritical CO_2 for 4 (a), 8 (b), and 16 (c) weeks. The graphs underneath each micrograph show the Ca/Si (blue) and Mg/Ca (green) elemental ratios measured along the micrographs using EDS.

layer, growing both outwards from the sample and inwards from the mould. It is mainly composed of Al-(hydr)oxides. When this coating is removed, the underlying sealant material is dark grey. In the outer ~700 μm of the sealant cylinder, the Si/Al, Ca/Al and Ba/Al ratios are elevated by about 1.2 to 1.3 times, suggesting a reduced Al-content. The Si/Al, Ca/Al and Ba/Al elemental ratios in the centre of the unexposed reference sample (i.e., on the map shown in Fig. 18a) are 0.62, 0.36, and 0.11, respectively.

3.5.2. *S4 exposed to CO_2-saturated water*

Exposure of S4 samples to CO_2-saturated water lead to some minor bleaching, mostly along the sample edges. After 16 weeks exposure, some local powdery precipitation was found on the sample surface. The SEM micrographs presented in Fig. 20 show that exposure to CO_2-saturated water for up to 16 weeks did not induce any significant microstructural changes in these samples. The EDS analyses presented likewise show no significant impact after 4 or 8 weeks exposure, while in the sample exposed for 16 weeks, a decrease in the Si/Al- and Ca/Al-

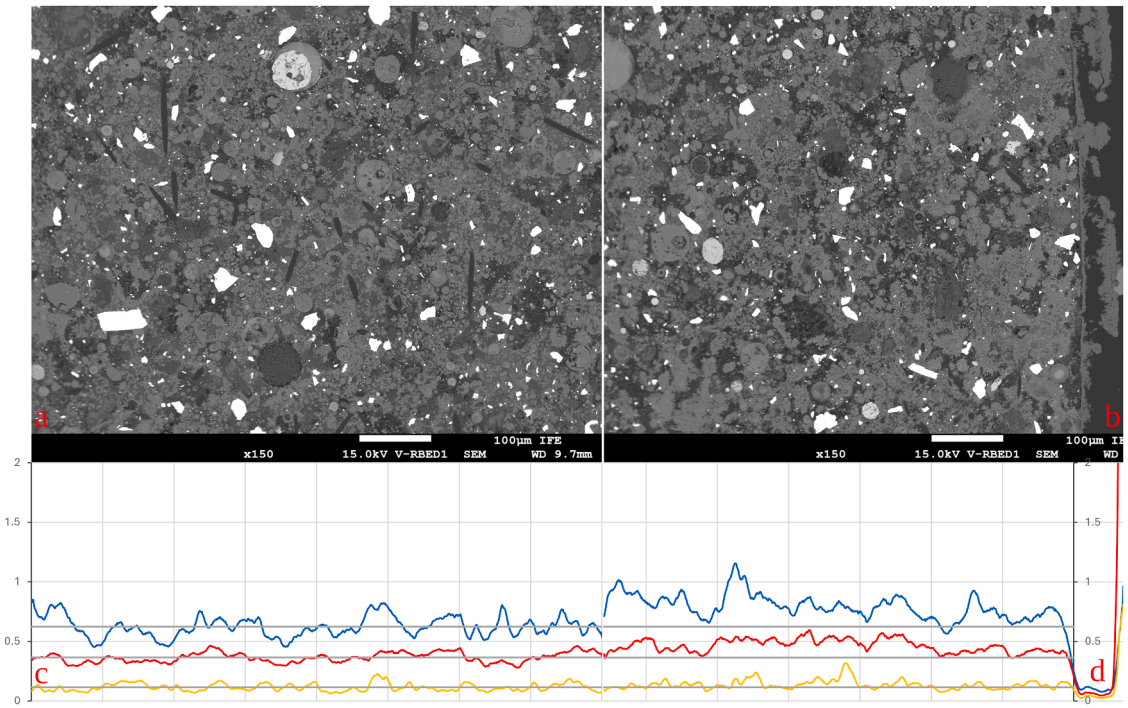

Fig. 18. SEM micrographs imaging a radial cross-section through an unexposed reference sample of S4, showing a) the centre of the sample, and b) the edge of the sample. Shown below the micrographs are the Si/Al (blue), Ca/Al (red), and Ba/Al (yellow) elemental ratios plotted against horizontal location in each micrograph.

ratios is observed at the sample edge, with these ratios then rising sharply from the sample edge to about 80 µm into the sample. As both the Ca/Si-ratio and the Ba/Al-ratio remain constant up to the edge of the sample, this suggests a depletion of Ca and Si at an approximately stoichiometric ratio.

The negligible impact of exposure to CO_2-saturated water observed in these samples is supported by the CT-scan (see Fig. 19), which likewise shows no significant change in density, except for some minor, localised reductions in density in the outer 80–120 µm. EDS-mapping shows a minor decrease in Ca/Al-ratios at the centre of all exposed samples.

3.5.3. *S4 exposed to wet supercritical CO_2*

S4 samples exposed to wet supercritical CO_2 showed some minor bleaching, mostly at the edges of the samples, and locally along the surface. Otherwise, no significant changes were observed optically. Exposure to wet supercritical CO2 likewise had little impact on the microstructure of S4, as can be seen in the micrographs presented in Fig. 21. After 4 weeks of exposure, a minor decrease in porosity may be seen in the outer ~20 µm of the sample, along with a small drop in Si/Al- and Ca/Al-ratios here. No significant effects are observed in the sample exposed for 8 weeks. Similar to the 4-week exposed sample, the 16-week exposed sample shows minor densification along the sample surface, here associated with a somewhat larger decrease in the Si/Al- and Ca/Al-ratios in the outer ~50 µm of the sample, caused by a minor increase in the Al-content in this zone. Inwards from this, the Ca/Al-ratio increases sharpy, and then decreases gradually from 50 to ~350 µm, though with very strong, sudden variations caused by localised areas with high Ca-content in matrix material with a harder, less-porous appearance.

CT scans of the S4 sample exposed to supercritical CO_2 (see Fig. 19) also shows no significant change in density, except for very minor, and not fully continuous density increases in the outer ~100 µm of the sample, as well as some localised area of increased density that may be the high-Ca matrix areas identified in the SEM images. EDS-mapping does not indicate any significant decrease in Ca/Al-ratios at the centres of the exposed samples.

3.6. *Microstructural alteration of sealant S5*

3.6.1. *S5 unexposed reference sample*

Freshly removed from the mould, S5 sample cylinders are covered by a thin, smooth layer of white precipitate. Once this is removed, the material underneath consists of a (relatively) light grey matrix, in which

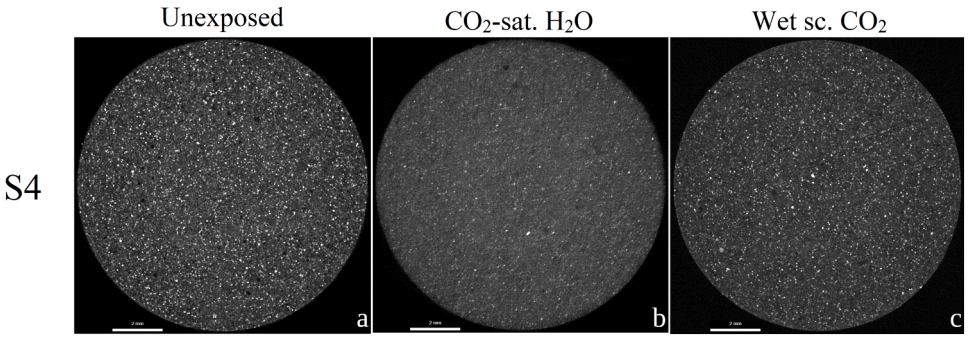

Fig. 19. CT-scans of sealant S4; unexposed, exposed to CO2-saturated water for 16 weeks, and exposed to wet supercritical CO2 for 16 weeks.

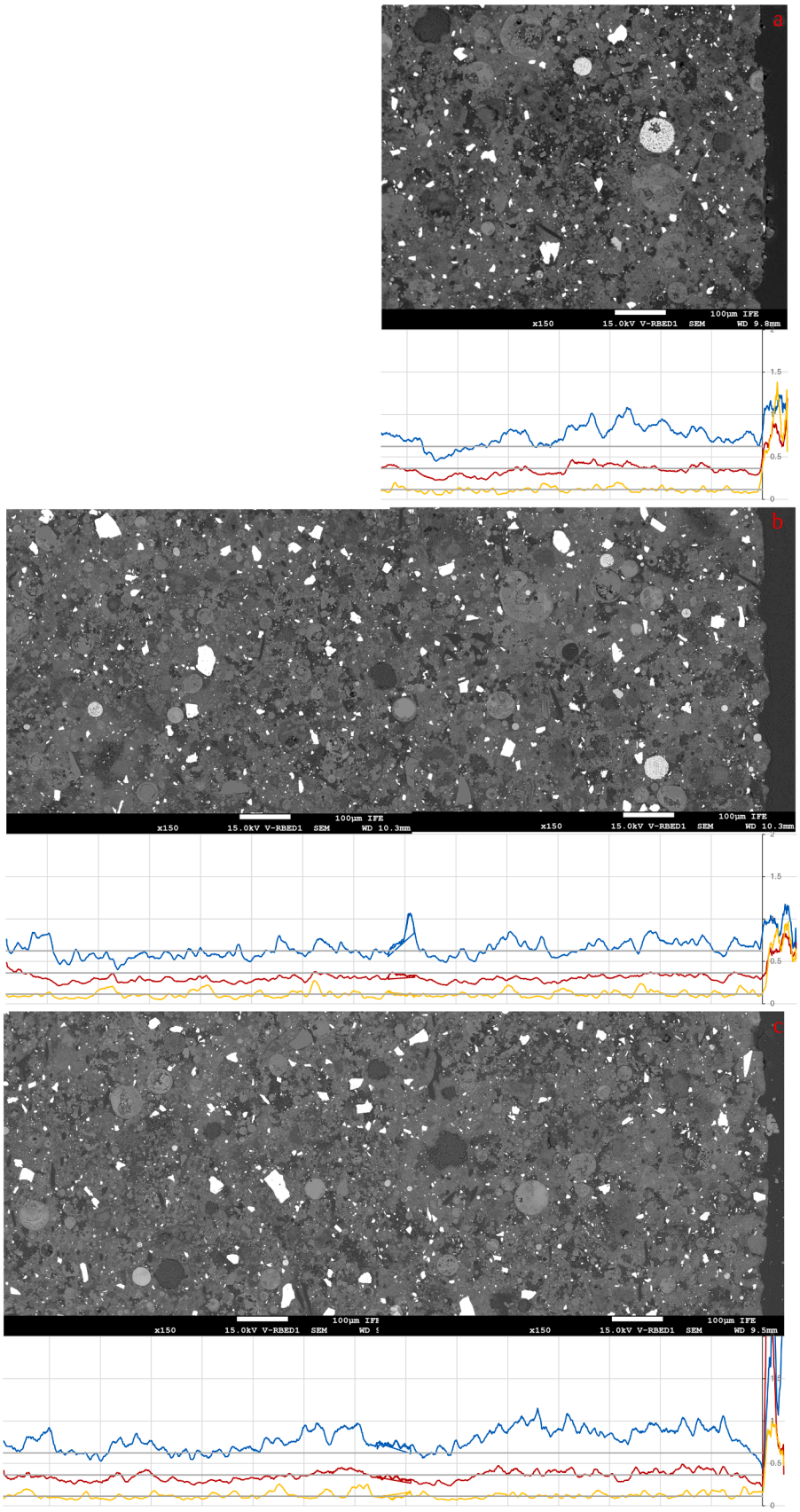

Fig. 20. SEM Micrographs of S4 samples exposed to CO_2-saturated water for 4 (a), 8 (b), and 16 (c) weeks. The graphs underneath each micrograph show the Si/Al (blue), Ca/Al (red), and Ba/Al (yellow) elemental ratios measured along the micrographs using EDS.

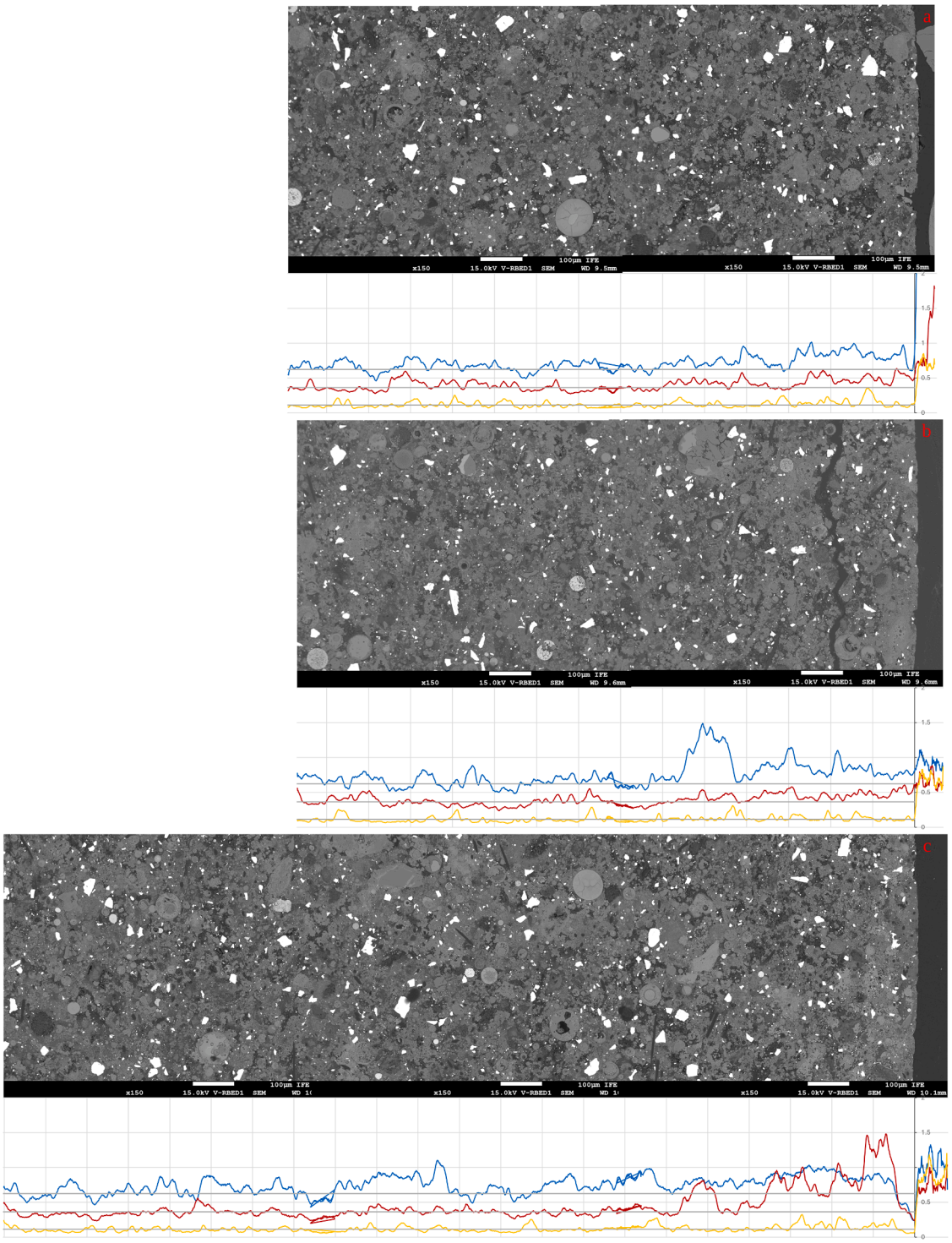

Fig. 21. SEM Micrographs of S4 samples exposed to wet supercritical CO_2 for 4 (a), 8 (b), and 16 (c) weeks. The graphs underneath each micrograph show the Si/Al (blue), Ca/Al (red), and Ba/Al (yellow) elemental ratios measured along the micrographs using EDS.

lighter and darker individual mineral grains can be seen with the naked eye. SEM micrographs of a cross-section through a reference sample of S5 (Fig. 22) show a high content of angular silicate grains embedded in a fine porous matrix. While most of these grains are below 100 μm in size, some are significantly larger than that. The matrix surrounding these grains is somewhat heterogeneous in competence, as can be seen from the darker areas that appear to be softer and more porous. Based on EDS-mapping, these contrasts are not correlated to any differences in chemical composition of the matrix, and they may represent degrees of hydration, or differences in gel microstructure (porosity). On the outer surface of the sample (Fig. 22b), a ~40 μm thick precipitate is observed, composed mostly of Ca-silicate with a fine texture of intergrowing, acicular crystals. The matrix material in the outer ~500 μm is again heterogeneous in competence, but strong compositional trends are not observed. The average Ca/Si, Mg/Si, Al/Si elemental ratios of the un-exposed reference sample (as measured on the centre map shown in Fig. 22a) are 0.32, 0.20, and 0.24, respectively.

The CT scan of the unexposed sample (see Fig. 23) shows an outer

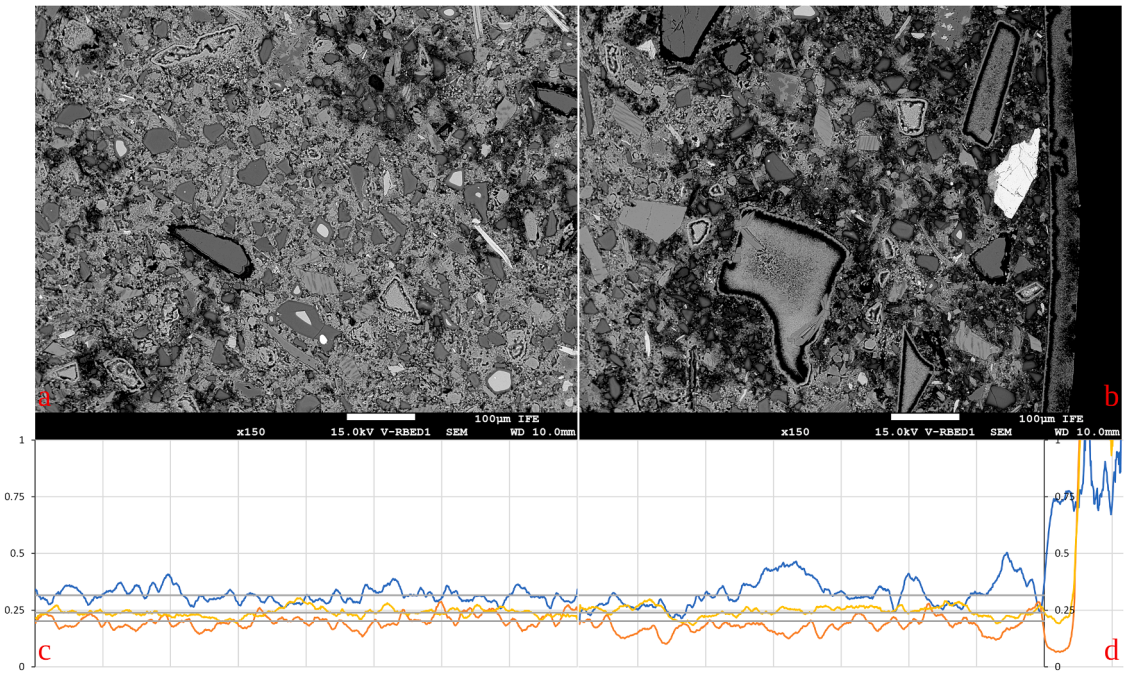

Fig. 22. SEM micrographs imaging a radial cross-section through an unexposed reference sample of S5, showing a) the centre of the sample, and b) the edge of the sample. In c) and d), plots of the elemental ratios of Ca/Si (blue), Mg/Si (orange) and Al/Si (yellow) are shown against horizontal location in the micrographs are shown as overlays in images.

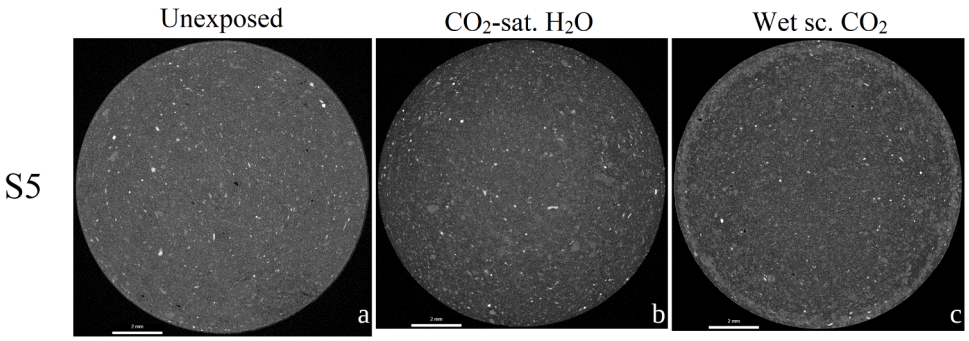

Fig. 23. CT-scans of sealant S5; unexposed, exposed to CO_2-saturated water for 16 weeks, and exposed to wet supercritical CO_2 for 16 weeks.

precipitate rim of about 50 µm thick, which can locally be seen to consist of two separate layers with some open spacing between them. Inwards of that, the outermost thin rim of the sample (about 50–60 µm wide) is elevated in density, while in general the sample matrix is not entirely homogeneous in density. This could be indicative of incomplete mixing. This matrix surrounds larger grains with higher density, as well as some larger, angular pores, that appear to have formed through the dissolution of solid grains in the hardening material.

3.6.2. *S5 exposed to CO_2-saturated water*

S5 samples exposed to CO_2-saturated water showed a slight yellow discolouration, but were otherwise similar in colour to the unexposed reference material. However, after dry storage, some samples were covered with a white layer that was strongly hygroscopic. Some larger crystals were observed on the samples, as well as in the vessel. Considering the SEM micrographs of S5 samples exposed to CO_2-saturated water shown in Fig. 24, some variability in matrix density is again observed, similar to that seen in the starting sample. Further decreases in density, indicating potential degradation, are observed towards the edges of the samples. In the 4-week sample, a continuous darker outer rim is observed with a width of about 60 µm, but otherwise, no specific CO_2-affected zones are identified based on microstructural variations. Considering the chemical analyses presented, the sample is depleted in Ca/Si. While this is most notable in the outer ~400 µm, the Ca/Si-ratio only increases gradually, and is still somewhat depleted at ~1.5 mm from the sample edge. The Mg/Si ratio is likewise somewhat depleted in the cross-section shown, and is also somewhat depleted at the centre of this sample (0.18 vs. 0.20 in the unexposed reference sample). Finally, an increase is observed in the Al/Si-ratio in the outer ~150 µm of the sample.

In the 8-week exposed sample, microstructural variations are similarly limited, with some heterogeneity in matrix competence, and a somewhat darker outer rim ~100 µm in width but no other clear trends with depth from the sample surface. Ca/Si-ratios show a more significant depletion along the full section shown. While this Ca/Si-ratio increases rapidly from ~1200 µm from the edge, this is ascribed to the presence of a large bubble filled with Ca-bearing phases (giving a local Ca/Si-ratio higher than 4). Mg/Si-ratios are likewise depleted more strongly than in the 4-week exposed sample. At the centre of this sample, however, Ca/Si-ratios are equal to those measured in the starting material, while Mg/Si-ratios are again depleted (0.18). A minor increase in Al/Si-ratio in the outer 100 to 200 µm of this sample may be correlated

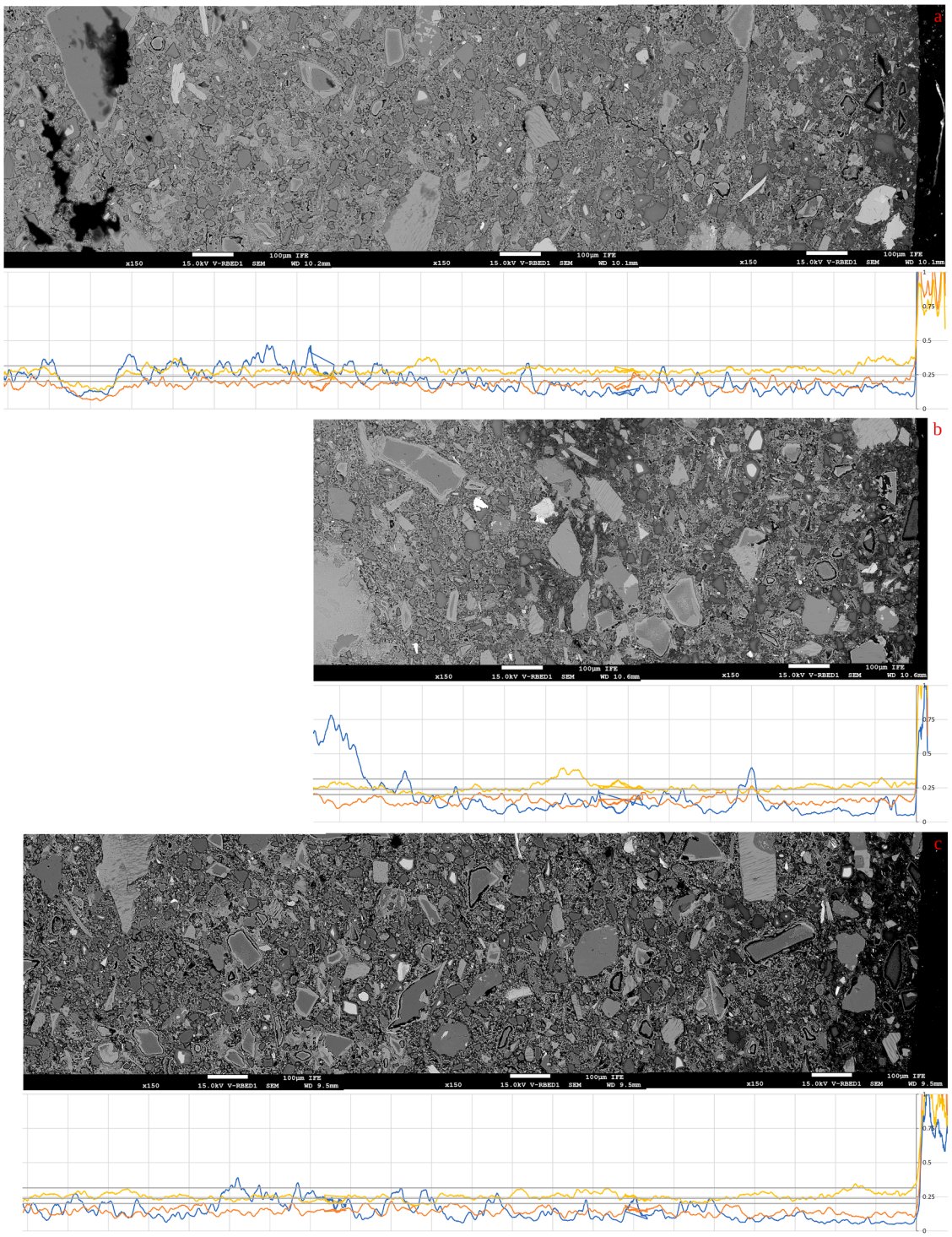

Fig. 24. SEM Micrographs of S5 samples exposed to CO_2-saturated water for 4 (a), 8 (b), and 16 (c) weeks. The graphs underneath each micrograph show the Ca/Si (blue), Mg/Si (orange), and Al/Si (yellow) elemental ratios measured along the micrographs using EDS.

to the occurrence of some larger Al-silicate grains here.

Finally, the 16-week exposed sample has a considerably darker rim in the outer 200 μm of the sample. Other than that, no microstructural variations are observed in this sample. Ca/Si and Mg/Si ratios are depleted to about 2260 μm from the edge, and somewhat more strongly than in the samples exposed for 4 and 8 weeks, indicating that continued exposure lead to increased removal of Ca and Mg from the sample, relative to Si. A minor increase in Al/Si is again observed in the outer ~200–250 μm of the sample. At the centre of this sample, both the Ca/Si-ratio (0.29 vs. 0.32) and the Mg/Si-ratio (0.15 vs. 0.20) are considerably depleted.

In the CT-scan of the 16-week exposed sample (see Fig. 23), three different zones can be identified based on density contrasts. In an outer zone of 1300 to 1400 μm wide, the sample matrix has a lower density than at the centre of the scan. The transition between these two different density zones is quite irregular, and takes place over a ~ 1200 μm wide transition zone. EDS-maps taken at the centres of the samples exposed for 4 and 8 weeks showed no significant change in Ca/Si-ratios, while

near the centre of the sample exposed for 16 weeks, the Ca/Si-ratio was somewhat lower than the unexposed reference value.

3.6.3. S5 exposed to wet supercritical CO_2

Samples of S5 exposed to wet supercritical CO_2 were mostly similar grey in colour as the starting material, but locally discoloured to be either lighter or darker. Fine white precipitates were observed locally, mostly around sample edges (where water might have been trapped between sample surface and sample holder) but also on the sample surfaces. Some of the S5 samples exposed to wet supercritical CO_2, after having been stored dry, also became covered in a white outer layer that is highly hygroscopic. The SEM micrographs of the sample exposed to supercritical CO_2 for 4 weeks, shown in Fig. 25, shows some degradation in the outer ~40 μm. EDS mapping shows depletion of the Ca/Si-ratio in the outer 200 μm, though most notably in the outer ~50 μm.

Similarly, the 8-week exposed sample shows a dark outer zone, indicating reduced density and thus competence of the matrix, that is roughly 100 μm wide. Within this, a relatively hard matrix with increased density, is observed for ~100 μm, anchored by a large open particle. Inwards from this, the matrix is darker again, indicating lower

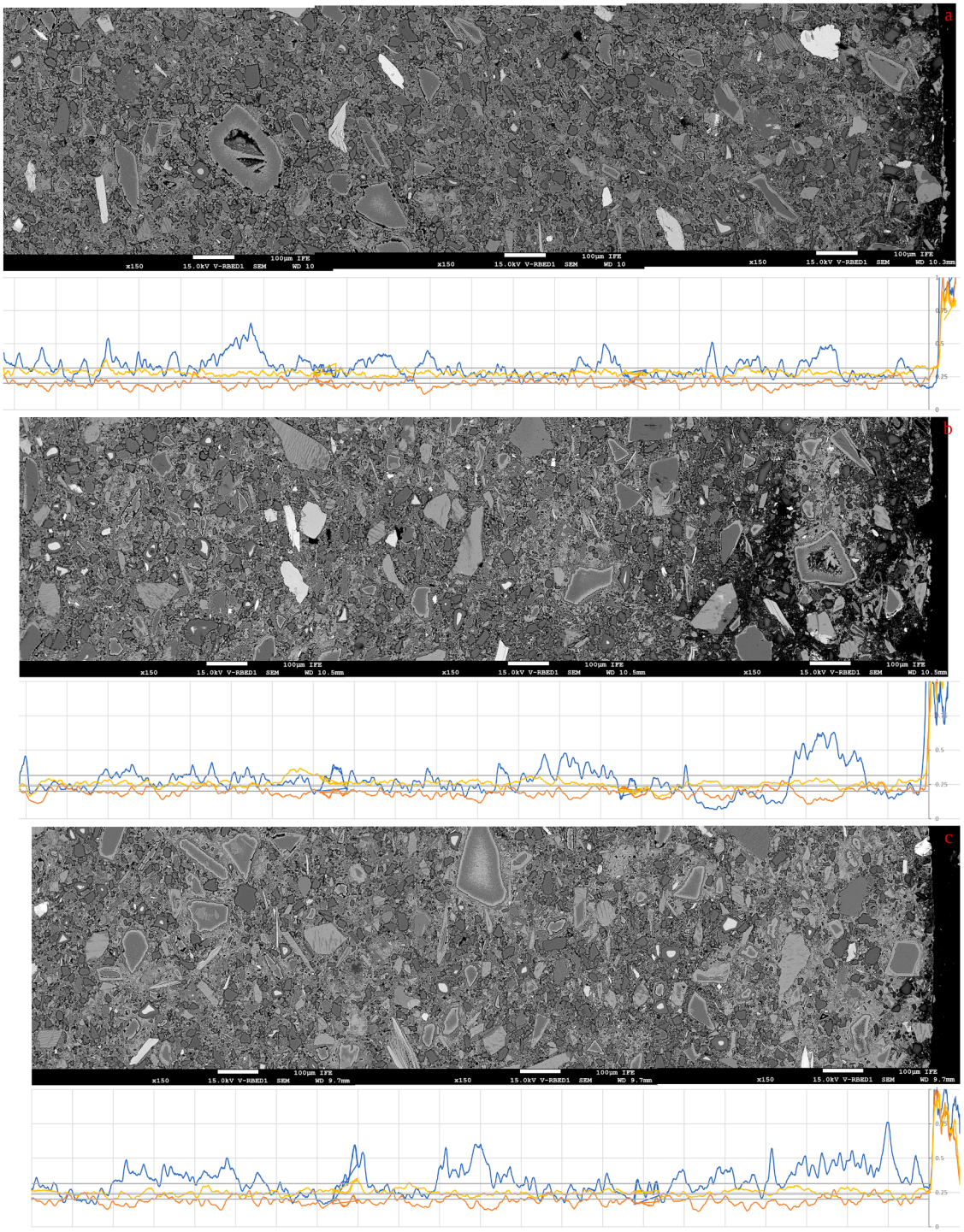

Fig. 25. SEM Micrographs of S5 samples exposed to wet supercritical CO_2 for 4 (a), 8 (b), and 16 (c) weeks. The graphs underneath each micrograph show the Ca/Si (blue), Mg/Si (orange), and Al/Si (yellow) elemental ratios measured along the micrographs using EDS.

competence. Here, the Ca/Si-ratio is relatively low to about 600 μm from the sample edge. Further inward, the matrix continues to show heterogeneity in competence and (thus) greyscale in the BSE micrographs. These variations in the matrix are associated with some fairly strong variations in Ca/Si-ratio, as well as some variation in the Mg/Si-ratio. Overall, the Ca/Si-ratio is somewhat depleted in this sample, even at the centre of the cross-section (0.28), as is the Mg/Si-ratio. Larger variations in matrix density or competence seen here are similar to the differences observed in the unexposed starting sample. However, in the starting material these variations were not associated with variations in chemical composition. One possibility is that these areas with relatively soft and porous matrix materials acted as conduits for CO_2-penetration, and the transport of dissolved cations.

The sample exposed for 16 weeks has a thin outer rim (<20 μm) with enhanced porosity, indicating removal of material. Here, the Ca/Si-ratio is similar to the starting ratio, but lower than measured nearby. Inwards from this rim, a zone is observed where the matrix appears hardened, with reduced porosity. These differences in matrix porosity are heterogeneously distributed, but observed down to ~500 μm into the sample, and are associated with a relatively high Ca/Si-ratio, as well as a very minor increase in the Mg/Si-ratio. Inwards from this, the material appears somewhat affected, with a reduced Ca/Si-ratio to a depth of about 960 μm. At the centre of the sample, the Ca/Si- (0.28) and Mg/Si-ratios (0.18) are both depleted relative to the unexposed reference sample.

The key observation in the CT-scan of the sample exposed to wet supercritical CO_2 for 16 weeks (see Fig. 23) is a mostly consistent rim with increased density between 170 and 510 μm from the sample edge, and negligible reduction in density inwards from 510 to 910 μm. Outwards of this rim, a similar matrix density is observed as in the core of the sample, though with some localised densification. The inwards bounds of the densified zone are sharply marked, but irregular. While the matrix directly adjacent to the densified material may be locally enhanced in porosity, mostly the sealant sample appears unaltered here. EDS maps taken at the centres of the exposed samples showed minor decreases in Ca/Si-ratios.

4. Discussion

Samples of five different sealants have been batch-exposed to CO_2-saturated water and wet supercritical CO_2 for up to 16 weeks, at 80 °C and 10 MPa. The impacts of exposure have been assessed using a range of analysis techniques, including mass change, fluid chemical analysis, testing with phenolphthalein, SEM, EDS, and CT-scanning. When evaluating the impact of CO_2-exposure on a sealant material, it is important to distinguish between CO_2-ingress, carbonation, and sealant degradation (cf. Zhang and Bachu, 2011). While CO_2 or CO_2-saturated water may penetrate deeply into sealant materials, as long as this ingress does not result in any significant chemical or physical changes in the material and the sample permeability is suitably low, this penetration may be considered of negligible importance. However, in materials that are (chemically) affected by CO_2, such as most OPC-based materials, inhibiting CO_2-penetration, for example by reducing sealant porosity and permeability, can be a mechanism for improving sealant durability.

Carbonation can be described as the precipitation of carbonates (most commonly, but not exclusively, calcite) through interaction between the intruding CO_2 and the sealant material (via a hydrous pore fluid). As this precipitation typically leads to a reduction in porosity and permeability, it is often considered to improve sealant quality and durability, and this process has even been considered and studied as a mechanism for self-sealing (or even self-healing) of sealants (Abdoulghafour et al., 2016, 2013; Liteanu and Spiers, 2011; Nakano et al., 2017; Wolterbeek et al., 2016). However, the carbonates precipitated during carbonation may in turn dissolve again when the pore fluid pH becomes too low, for example due to prolonged exposure to CO_2, in particular when the sealant is also exposed to a large or flowing volume of water (cf. Hernández-Rodríguez et al., 2017). Furthermore, carbonation will change the pore fluid composition (notably lowering the Ca^{2+}-concentration and may in turn drive dissolution and leaching of Ca^{2+} and other cations from deeper parts of the sealant. This dissolution and leaching can cause changes in the material properties of the sealant, as it may lead to an increase in porosity and permeability, and a loss in mechanical integrity. In particular, in OPC-based sealants, significant degradation starts to take place once all $Ca(OH)_2$ is dissolved, and further Ca^{2+} is released through leaching and dissolution from the CSH-gel and/or dissolution of precipitated $CaCO_3$. Thus, while carbonation itself may be beneficial, it can also be a precursor to degradation. Accordingly, harnessing carbonation to restrict further penetration of CO_2 into the sealant material, for example through the addition of components that react with CO_2 to form chemically more stable carbonates (e.g., Mg-silicates to form magnesite, $MgCO_3$), can be another mechanism for improving sealant durability, as long as subsequent degradation upon prolonged exposure can be avoided.

While testing with phenolphthalein has shown that all sealant samples tested (diameter 12 mm) were fully affected by exposure to CO_2 already after 4 weeks, leading to full dissolution of all $Ca(OH)_2$ (and hence the drop in pH observed), and decreases in Ca/Si-ratios, associated changes in microstructure at the sample cores were limited. While similar depths of CO_2-penetration have also been observed in other batch tests (e.g., Barlet-Gouédard et al., 2006; Duguid and Scherer, 2010; Kutchko et al., 2009; Lesti et al., 2013; Todorovic et al., 2020 for various sealant compositions based on Class G and Class H cements), others report slower carbonation (e.g., Kutchko et al., 2008; Lesti et al., 2013 for neat Class G or Class H cement). However, it should be noted that, with the exception of (Lesti et al., 2013), these studies do not include testing with phenolphthalein.

More significant impacts due to alteration and degradation can be observed using SEM and CT (density changes, and other changes in microstructure), and EDS (significant changes in chemical composition as tracked through elemental ratios). For all samples, these extents of alteration and degradation, as indicated by microstructural observations and elemental composition ratios, are displayed in bar diagrams in Fig. 26.

Though for most compositions and exposures, the depth of degradation (due to carbonate dissolution – Zhang and Bachu, 2011) is not clearly correlated to exposure time, suggesting potential healing of sealant microstructures (e.g., in S1 exposed to CO_2-saturated water), or some reaction limiting mechanism, the depth to which the microstructures and chemical compositions are otherwise altered does often show a correlation to exposure duration. These correlations can be expressed as a power law, where the depth to which the material is altered (D_a in m) depends on exposure duration (t in y) with exponent x, and constant C:

$$D_a = t^x \times C$$

Values for the constants for the compositions tested (except for S4, where very little to no effect of exposure was observed are given in Table 3. Based on the constants derived, extrapolated depths of CO_2-impact after 30 years range from 1–140 mm for wet supercritical CO_2, and 2–260 mm for CO_2-saturated water. However, as these constants are based on a limited number of datapoints obtained in a batch-type study on a small number of samples, their reliability is limited. Furthermore, this notes the depth to which the samples showed signs of being affected by CO_2 in terms of microstructure and chemical composition – degradation depths were shallower, while testing with phenolphthalein indicated full $Ca(OH)_2$-depletion of our (12 mm diameter) samples already after 4 weeks.

The alteration depths after 30 years estimated here fall within the range of 30-year alteration depths compiled by (Zhang and Bachu, 2011) for both wet supercritical CO_2 (1.7–180 mm) and CO_2-saturated water (1–723 mm), based on tests carried out at 50–90 °C.

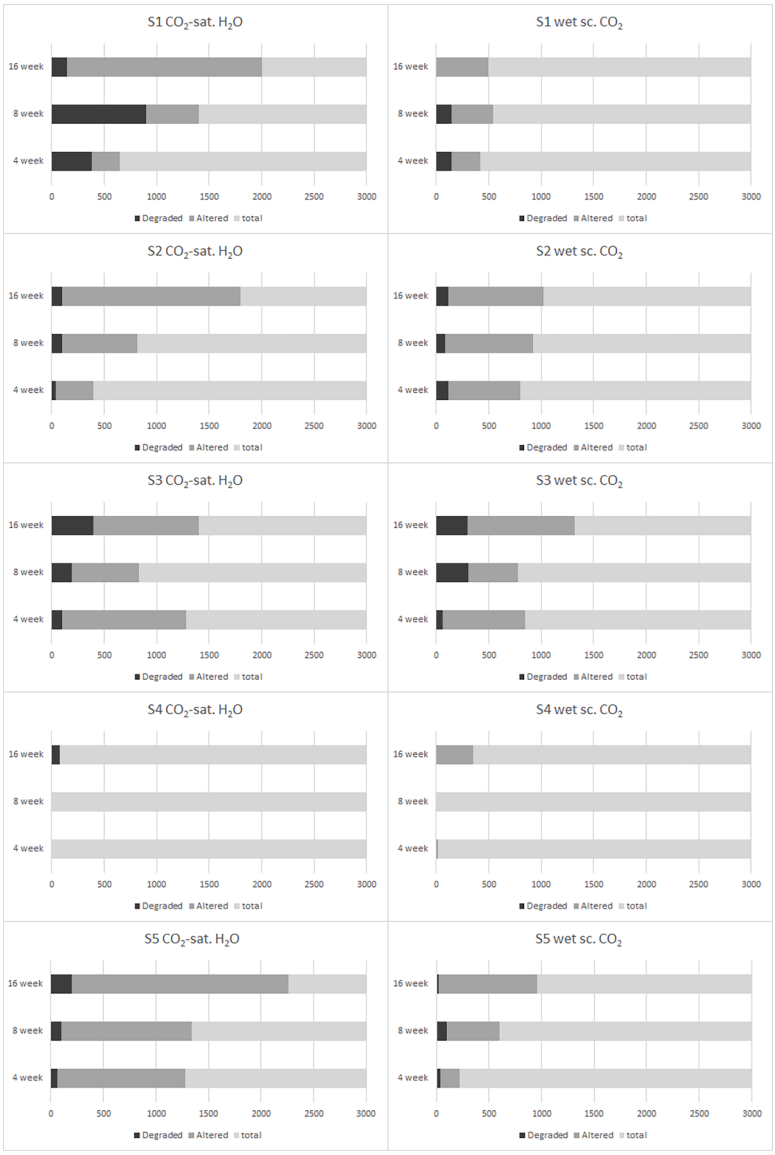

Fig. 26. Bar diagrams indicating the depths of degradation and the depth to which sealants were altered by CO_2-exposure based on SEM micrographs, elemental ratios, and CT-scanning. "Degraded" indicates the depth to which the material is visibly degraded as a result of exposure to CO_2, with elevated porosity, lowered mechanical competence, and (in some cases) strongly altered chemical composition (e.g., Ca/Si-ratio). "Altered" indicates the depth from which the material appears unaltered by CO_2, based on microstructure and assessed elemental ratios. Note that testing with phenolphthalein has indicated complete dissolution of $Ca(OH)_2$ from all exposed samples (except S4, where testing with phenolphthalein is not relevant).

Table 3
Fitting constants for extrapolation of alteration depth due to exposure to CO_2, and extrapolated 30-year alteration depths.

	Wet supercritical CO_2			CO_2-saturated water		
	x	C	30-yr depth (mm)	x	C	30-yr depth (mm)
S1	0.126	0.61×10^{-3}	0.94	0.811	5.58×10^{-3}	88
S2	0.175	1.26×10^{-3}	2.3	1.08	6.42×10^{-3}	257
S3	0.318	1.74×10^{-3}	5.1	0.065	1.29×10^{-3}	1.6
S5	1.06	3.69×10^{-3}	137	0.410	3.39×10^{-3}	14

4.1. S1

Exposure of S1 samples to CO_2-saturated water lead to considerable alteration in these samples. While samples increased in mass during the first four weeks of exposure, the sample mass decreased during further exposure. Furthermore, considerable and increasing amounts of precipitation were observed on the outer surfaces of these samples after removal from the vessel. Fluid Ca-contents and Si-contents increased rapidly initially, but were stable from 8 to 16 weeks, suggesting $CaCO_3$, and silica saturation had been attained.

Interpretation of the SEM micrographs and Ca/Si-ratios indicates that most of the sample degradation took place the first 8 weeks of exposure. This degradation, seen as an increase in porosity and a reduction of the Ca/Si-ratio reached 400 and 900 μm deep, respectively. However, the sample exposed for 16 weeks was subsequently sealed by carbonation during the last 8 weeks exposure. Here, it should be noted that between the 4 and 8 week exposures, about 75 % of the exposure water had to be replaced, thus enhancing the dissolution potential, while

between 8 and 16 weeks only about 5 % of the exposure water was replaced. While no carbonation was confirmed in the 4-weeks exposure sample, in both the 8- and 16-weeks exposed samples, porosity-reduction through carbonate precipitation was observed down to a depth of 1150 μm, though considerably more prevalent in the 16-weeks exposed sample. The CT-scan confirmed this maximum depth of carbonation into the sample exposed for 16 weeks. However, beyond that, the material is affected by exposure to CO_2, with altered microstructure and a Ca-depleted zone (relative to Si) down to about 1900 to 2000 μm from the sample edge.

In the samples exposed to wet supercritical CO_2, some degradation was observed in the outer zone, to a depth of ~150 μm after 4 and 8 weeks of exposure, also indicated by a decrease in Ca/Si-ratio and some carbonation down to depths of 240 μm and 320 μm, respectively. In contrast, in the sample exposed for 16 weeks, carbonation was observed from the surface and to a depth of about 500 μm. In all these samples, carbonation was associated with an increase in the Ca/Si-ratio, though this is most significant for the 16-week sample.

4.2. S2

Sample mass changes of S2 samples exposed to CO_2-saturated water showed an increase after 4 weeks of exposure, followed by a slight decrease in mass after 8 and 16 weeks, and a similar trend was also observed in the samples exposed so wet supercritical CO_2. Fluid Ca-contents remained stable between 4 and 16 weeks of exposure, at a similar value as measured for S1, while Si-contents were lower and increased continuously, suggesting that while Ca-saturation was rapidly reached, Si-saturation was not reached during 16 weeks of exposure. Note that, as with S1, a large fraction (~44 %) of the exposure water was replaced after 4 weeks, while only a small sample (~5 %) was taken and replaced after 8 weeks.

These observations match SEM observations, that show that in samples of S2 exposed to CO_2-saturated water, degradation penetrated from 40 to 100 μm between 4 and 8 weeks exposure, but did not penetrate further after that. Carbonation, on the other hand, proceeded continuously, from 240 to 460 to 580 μm, while chemical alteration (based on Ca/Si-ratio) increased continuously, reaching a depth of 1800 μm after 16 weeks. For the 16 weeks exposed sample, similar microstructural changes were identified through CT-scanning.

In the samples exposed to wet supercritical CO_2, degradation was sharply delineated and limited to the outer 90–120 μm, relatively independently of exposure time. Inwards from that, carbonation resulted in densification and porosity reduction. While the intensity and width of the carbonated zone increases with increasing exposure duration, the depth to unaltered appearing material increases only little with exposure duration, from 800 to 1020 μm.

4.3. S3

While S3 is very similar in composition to S2, the replacement in S3 of 28.5 % of the binder with RePlug™, an olivine-based CO_2-sequestering additive, caused this material to behave quite differently upon exposure to CO_2. Previous studies on the exposure of olivine to water and CO_2 at pressures and temperatures similar to our experimental conditions have shown rapid dissolution of the olivine, with precipitation of magnesite and silica (cf. van Noort et al., 2013, and references therein). Accordingly, in the tests reported here the olivine is expected to provide Mg^{2+}, leading to the precipitation of Mg-carbonates (or Ca, Mg-carbonate, as considerable Ca^{2+} is also available). These carbonates should then clog the pore network similarly to calcite (or aragonite) in regular OPC-based sealants, restricting further penetration of CO_2 and inhibiting degradation. On the larger olivine grains seen in these samples, clear signs of such dissolution and subsequent precipitation were not observed. However, the added Mg-silicates had a wide grain size distribution, and the smallest grains were likely more reactive. Therefore, while based on the data available here, the direct extent and impact of olivine dissolution and Mg-carbonate precipitation cannot be assessed, this will be addressed in a future study. Analysis of the exposure fluid chemical compositions do show the release of considerable Mg into the exposure fluid, while Ca- and Si-contents in the fluids were relatively low compared to S1 and S2, suggesting that the added olivine did impact the release of Ca and Si. Samples masses increased after 4 weeks of exposure to either wet supercritical CO_2 or CO_2-saturated water, though somewhat less than for S1 and S2. After 8 and 16 weeks of exposure, sample masses had decreased somewhat, but were still higher than initial sample masses; similar to what was observed for S2.

In part due to its relatively low mechanical competence (cf. Li and Pluymakers, 2024b), preparing representative polished cross-sections through S3 samples was relatively difficult. Based on the cross-sections obtained, exposure to CO_2 lead to the formation of a new matrix microstructure, consisting of rounded islands. While deeper into the exposed samples, these islands are at a 10 s of μm scale, closer to the sample edges, they are much finer. In the carbonated parts of samples exposed to wet supercritical CO_2, this finer microstructure is further associated with a lower porosity. In the samples exposed to CO_2-saturated water, the insular particles in the altered zone have darker cores surrounded by lighter rims; the latter similar in colour (i.e., density) to the material found further inwards.

For the sample exposed to CO_2-saturated water for 16 weeks, the CT-scan shows localised degradation within the outer 200 μm of the sample, and then a zone of relatively low porosity to about 1500 to 1900 μm from the edge. SEM imaging shows an outer zone with relatively high porosity that is about 400 μm wide, somewhat wider than seen in the CT-scan. Inwards of that, carbonation effects on sample composition and microstructure were identified down to about 1400 μm; somewhat shallower than assessed based on the CT-scan, though it should be noted that the changes in microstructure and density identified here are quite gradual. SEM imaging of the samples exposed for 4 and 8 weeks indicates that the degraded outer rim increased in width continuously (at about 25 μm per week), while other microstructural changes did not show strong correlation with exposure duration.

For the sample exposed to wet supercritical CO_2 for 16 weeks, both SEM and CT-scanning show localised degradation of the sample microstructure in the outer ~200 μm, and a continuous densification, associated with a dense, insular matrix in the SEM images, down to 1100 to 1320 μm. SEM images of samples exposed for 4 and 8 weeks suggest an increase in degradation (both depth and degree) with exposure time. Here, the 8-week exposure sample looks less altered than the 4-week exposure sample, which may be due to sample variability (within or between samples) or to surface preparation effects due to the relative low hardness of S3.

EDS measurements on samples exposed to either CO_2-saturated water or wet supercritical CO_2 show that the increased porosity in the outer zone is correlated with a depleted Ca/Si-ratios, while the Mg/Si-ratio is relatively unaltered.

4.4. S4

The analyses on exposed samples of S4 consistently show that exposure to either supercritical CO_2 or CO_2-saturated water for up to 16 weeks had very limited impact on this material. Sample masses in either exposure decreased negligibly. Here, as the mass measurements on samples exposed to sc. CO_2 for 4 weeks diverge strongly from all other measurements, it is assumed that these measurements were affected by a measurement error. Likewise, fluid chemistry measurements show low concentrations of Ca, and while Si-concentrations are relatively high compared to most other samples, total ion concentrations in the exposure fluids are still very low. SEM and CT-scans likely show very little impact of CO_2-exposure. Minor dissolution and leaching was observed at the edges of the sample exposed to CO_2-saturated water, though this dissolution may not have been affected by the presence of CO_2. Exposure

to wet supercritical CO_2 lead to densification (carbonation) in a narrow outer rim, but otherwise had limited to no impact on sealant microstructure and integrity.

4.5. S5

The microstructural impacts of exposure on S5 sealant samples are somewhat obfuscated by pre-existing sample variability and heterogeneity, potentially indicating incomplete mixing of these samples, or separation of the material during or after casting. Exposure to CO_2-saturated water led to significant decreases in sample mass after 8 and 16 weeks, associated with the leaching of, in particular, K, as well as Mg and Si. Note that the sample mass increase after 4 weeks, as well as the fluid chemical analyses, may have been impacted by contamination from the vessel, as this vessel had been used previously. SEM imaging likewise shows sample degradation at the surface of the sample, with the degraded zone widening quite linearly with increasing exposure duration, while the degree of degradation appears to worsen. EDS analyses show this to be correlated to depleted Ca/Si- and Mg/Si ratios. Here, it should be noted that some degree of depletion is observed throughout these samples, and may indicate full alteration of these samples, though pre-existing sample variability (between the reference sample and exposed samples) cannot be fully excluded. The CT-scan of the sample exposed for 16 weeks likewise shows a somewhat lower matrix density, interpreted as minor degradation, down to about 2.5 mm into the sample, which correlates with a depleted Ca/Si-ratio observed in SEM to about 2.3 mm from the sample edge.

In contrast, the samples exposed to wet sc. CO_2 showed little change in sample mass. The sample exposed for 4 weeks showed some degradation in the outer ~40 μm in the SEM, along with some depletion in the Ca/Si-ratio in the outer ~200 μm. The sample exposed for 8 weeks showed some variability in gel density in the outer ~300 μm. As a low density in the outer ~100 μm was associated with a low Ca/Si-ratio there, this may indicate degradation. The elevated gel density observed locally between 100 and 200 μm may represent carbonate-precipitation. While the gel density is relatively low between 200 and 300 μm, here the Ca/Si-ratio is elevated, and thus this could reflect inhomogeneity of the sample. Reduced Ca/Si-ratio and altered microstructures were observed down to about 600 μm. SEM images of the sample exposed for 16 weeks and the CT-scan of that sample both show localised degradation in the outer ~20 μm, followed by significant densification, down to about 510 μm into the sample. This carbonation is associated with a relatively high Ca/Si-ratio, and a somewhat elevated Mg/Si-ratio. Within that zone, a minor decrease in density is associated with a reduced Ca/Si-ratio to a depth of about 960 μm. Furthermore, the Ca/Si- and Mg/Si-ratios in these samples are not depleted as those in the samples exposed to CO_2-saturated water, showing the impact of leaching and exposure to (relatively large volumes of) water on these sealants.

4.6. Enhancing long-term sealant durability through different mechanisms

Comparing the behaviour of the different sealants tested here (in particular to reference sample S1), the different mechanisms that were used in designing these sealants to improve their long-term durability can now be analysed and discussed. S2 mainly differed from S1 in the addition of silica fume and MgO aimed at strongly reducing its matrix porosity and permeability. Note that these changes in composition will have also changed the reactivity of this sealant, in particular by reducing the availability of free lime ($Ca(OH)_2$) as the Ca/Si-ratio was reduced (from 1.1 to 0.94). Indeed, our measurements show less strong mass changes for S2 than for S1, while changes in fluid chemistry were also somewhat limited, indicating that S2 was more resistant to leaching and dissolution. In particular, the Si-contents in the S1 fluids were higher than in the S2 fluids, despite S1 having a higher Ca/Si-ratio, confirming that S1 was more vulnerable to dissolution than S2.

This observation is further supported by the microstructural analyses on S1 and S2, made using SEM and CT-scanning, which show that the outer, degraded zone is considerably narrower in exposed S2 samples compared to exposed S1 samples. However, densification ascribed to carbonate precipitation is seen to similar depths in both sealants exposed to CO_2-saturated water, and to somewhat greater depth in the S2 samples exposed to wet sc. CO_2 than in the S1-samples similarly exposed. Furthermore, testing with phenolphthalein has shown complete dissolution of $Ca(OH)_2$ from all exposed samples of S1 and S2. These observations suggest that while the reduced porosity and permeability may limit dissolution and degradation at the outer surface of a sealant volume, they may not (significantly) restrict the penetration depth of alteration when a sample is exposed to wet sc. CO_2 under hydrostatic, batch conditions where there is no pressure gradient driving CO_2-ingress into the sample, and ingress is thus controlled by diffusion. Here, it should additionally be noted that the lower porosity and lower free lime content likely mean that less CO_2 is needed for full carbonation, and for occupying all gel porosity, and that while the CO_2-ingress depth may be somewhat larger, the total mass of CO_2 that penetrated into the S2 samples may be lower. (Brunet et al., 2013) present a reactive transport model in which the alteration depth of Class H cement samples exposed to CO_2-saturated brine is dependent on the initial porosity and portlandite content, In this model, low porosity and high portlandite content lead to a narrow, dense calcite precipitation zone, but also strong degradation outside that zone, while high porosity and low portlandite content lead to a wider calcite zone with greater alteration depth, but less degradation at the interface, comparable to the differences observed here between S1 and S2. In addition, there was much less carbonate precipitation on the outer surface of S2 samples (exposed to CO_2-saturated water) than on S1 samples exposed similarly, further demonstrating the much lower overall reactivity of S2.

S3 differs from S2 by the replacement of a significant portion of the OPC-based binder with olivine (as RePlug^{TM}). This olivine was mainly added to harness its carbonation potential to reduce sealant porosity and permeability while forming a more stable reaction product (e.g., magnesite or dolomite) when exposed to CO_2. However, the replacement of a significant portion of the binder with powdered olivine caused considerable changes in hardened sealant microstructure, mechanical properties, and in how the sealant reacted upon exposure to CO_2 compared to more conventional OPC-based sealants (i.e., S1 and S2). In particular, while the depth of degradation in the S3 samples was deeper than in the S2 samples, the degree of degradation, especially in the samples exposed to CO_2-saturated water, was less severe. This corresponds well to the model of (Brunet et al., 2013), but may also further suggests that the added mineral component did indeed protect the sealant from degradation due to CO_2-exposure. This is also supported by fluid chemistry analyses showing considerably lower Ca-contents in the fluids in which S3 samples were exposed compared to S2. Note, that based on the Ca/Mg-ratio in these fluids, and assuming that the fluid composition was representative for the sample pore fluids (i.e., no local variations in pore fluid chemistry), the stable carbonate forming in S2 would have been dolomite, while either magnesite or dolomite would have been stable in S3 (Marini, 2007). However, exploring the exact impact of the olivine added to this sealant will require a deeper microstructural investigation, which will be addressed in a future publication.

Comparing the effects of CO_2-exposure on S1, S2 and S3 thus allows us to assess the efficiency of different mechanisms for improving sealant durability applied in these OPC-based sealants. Compared to S1, S2 was formulated to have a reduced porosity and permeability, to inhibit the penetration of CO_2 into the sealant material. Interestingly, while the reduced permeability was successful in limiting degradation, in these batch exposure experiments, where CO_2-penetration into the sealant samples took place by diffusion rather than flow driven by a pressure gradient, the reduced permeability did not lead to reduced alteration depths. This comparison thus shows that developing a sealant to have a reduced permeability (and porosity) by adding reactive silica fume and MgO can be a successful strategy to develop a sealant that is more

resilient against CO_2-exposure. However, the individual impacts of permeability-reduction and the lower Ca/Si-ratio due to silica-addition should be taken into account separately. Here, it is interesting to note that (Lesti et al., 2013) report improved resistance to carbonation-induced degradation for a cement system based on a CEM III/A further amended with reactive electro filter fly ash to reduce the Ca/Si-ratio in the mix, and ensure excess SiO_2 was available to bind all Ca during curing.

Further comparing S2 to S3, the additional impact of harnessing carbonation to improve sealant properties can be assessed. Here, the addition of olivine further limited the degree of sealant degradation, if not the depth to which the material was degraded. However, based on the data obtained, it is not possible to assess whether this significantly improved the durability of S3 compared to S2 as this would require long-term experiments exposing these samples to (large volumes of) CO_2-saturated water to determine whether the carbonates precipitate did indeed have improved chemical resilience compared to carbonates precipitated in S2. The impact of permeability reduction on sealant durability may be more visible in forced-flow tests, where a flow of CO_2 or CO_2-saturated water is forced through sealant materials. Likewise, the durability of precipitated carbonation products in S3 samples may be better assessed in (long-term) flow-through experiments using CO_2-saturated water, as this provides a dissolution potential.

Sealant S4, to the contrary, was designed to have high chemical resistance when exposed to acidic conditions, including CO_2. Indeed, while exposure to CO_2-saturated water lead to some minor dissolution and degradation at the sample edge (mostly to saturate the water phase), exposure to wet sc. CO_2 lead to only minor alteration in the outer edges of the sample. Sample mass changes were negligible, further demonstrating the non-reactive nature of the sealant material.

The rock-based geopolymer S5 was designed specifically to have a low Ca-content, as well as a low porosity and permeability. While Ca can play a key role in the geopolymerisation process (especially in the early stages of polymerisation – cf. Hajiabadi, Khalifeh, van Noort, et al., 2023b, a low Ca-content was targeted in order to induce the formation of a geopolymer gel in which Ca was not a significant structural component, as it is in the CSH-gels formed during the hardening of OPC. Thus, the negative impact of Ca-leaching on sealant integrity would be mitigated. In addition, the GP was engineered to have a low permeability in order to limit CO_2-ingress. While our observations may have been obscured by sample inhomogeneity, it appears that exposure to CO_2-saturated water did lead to the leaching of K, Ca, Mg and other elements throughout our samples, as indicated by changes in the Ca/Si-ratio. However, based on CT-scans and SEM images, the resulting degradation of the GP material appears to have been limited, suggesting that this leaching did not significantly impact sample integrity. Exposure to wet sc. CO_2 led to clear, significant carbonation and densification in a relatively narrow outer rim (500 μm after exposure for 16 weeks), while after shorter exposure durations only limited carbonation and densification were observed. In these samples, leaching and degradation were localised, and limited to a narrow outer rim of the sample (in particular there were carbonation was observed), but the observed changes after different exposure durations were somewhat inconsistent, and may have been impacted by sample variability.

Sealant designs S4 and S5 show that it is possible to design a sealant to be non-reactive when exposed to CO_2 and water, or to have only limited reactivity. However, while such a sealant will not be affected chemically, leakage pathways may form nonetheless due to mechanical and/or thermal changes. When such leakage pathways do form, a non-reactive sealant will not have any self-sealing capacity. Therefore, it may be more beneficial to develop a sealant that is reactive when exposed to CO_2 (in the presence of water), but where such exposure does not lead to significant degradation of the sealant. The results obtained on our geopolymer sample (S5) suggest that a low-Ca geopolymer may indeed provide such a sealant. However, further studies assessing the impact of prolonged exposure (especially to CO_2-saturated water) are required to further ascertain whether the gel matrix of the GP will be able to sustain sealant integrity over longer durations. Furthermore, a more detailed study of the microstructure of the S5 samples exposed in this study may also improve our understanding of the mechanisms by which this material is affected by exposure to CO_2, which will in turn improve our ability to extrapolate the integrity of this sealant over the full duration required for GCS.

5. Future work

The work presented here shows that while most cementitious sealants tested were affected by CO_2, leading to full CO_2-penetration after only 4 weeks, as well as carbonation and even degradation at the outer surfaces, the degree and extent of, in particular, degradation could be reduced through changing the sealant composition. In all compositions tested, degradation was limited to the outer parts of the samples, though visible microstructural and chemical alterations penetrated more deeply. While the data was too variable, and experimental durations were relatively short, to perform a reliable extrapolation, the approximate extrapolated rates presented here indicate maximum alteration rates of (much) <1 cm per year, showing that all sealant compositions tested have good potential for maintaining wellbore integrity. Extrapolation to 30 years gave alteration depths in the range of 2–260 mm for CO_2-saturated water, and 1–140 mm for wet supercritical CO_2, comparable to the ranges reported in the literature (e.g., Kutchko et al., 2009, 2008; Zhang and Bachu, 2011). However, the results presented here show that the potential for maintaining long-term integrity may be further enhanced by reducing permeability (and porosity), by modifying the reactivity with a CO_2-sequestering agent (olivine), by developing a sealant in which Ca-leaching does not significantly impact the gel structure and integrity, or by using a sealant that is essentially non-reactive in the presence of water and CO_2. The result presented here thus provide important input when selecting sealants to be used in newly drilled wellbores, as well as for sealants to be used for plugging existing wells in reservoirs targeted for CO_2-injection. Furthermore, our results may also provide insight into how seals pre-existing wells in (depleted gas) reservoirs may resist exposure to CO_2 during CO_2-storage.

While the current research was carried out using pure CO_2, the presence of low concentrations of impurities may further impact wellbore seal integrity. Exposure experiments have now been carried out, where samples of the same five sealants are exposed to CO_2 containing low concentrations of H_2S and H_2SO_4 to assess how the presence of these impurities may impact these materials' interactions with CO_2.The results of these exposure experiments have been submitted for publication (van Noort et al Submitted). In addition, microstructural analyses on a more detailed scale than addressed here may provide better insights into the mechanisms by which these samples reacted with CO_2. Such more thorough analyses are especially relevant for sealants S3 and S5, where some of the reaction mechanisms are not yet fully understood based on the data reported here, and are currently ongoing. Finally, to fully understand how the results obtained here may extrapolate to long-term integrity, modelling of transport rates and reaction front velocities is required. Ideally, such modelling is supported by experiments with a wider range of exposure durations than were possible during this project.

As a final note, while the present manuscript addresses the ability of the five sealants to withstand exposure to CO_2-containing fluids, the suitability of any material as a sealant in GCS applications is also determined by other properties, such as mechanical behaviour, permeability, and the ability to withstand temperature changes. Therefore, to fully assess the suitability of any sealant for GCS, these properties, as well as the impact of CO_2-exposure on them, also need to be addressed.

6. Conclusions

In this study, five different cementitious materials were exposed to

CO_2-saturated water and wet supercritical CO_2 at 80 °C and 10 MPa, for durations of 4, 8 and 16 weeks. The sealants studied were an OPC-based reference sealant (S1), an OPC-based sealant modified for reduced porosity and permeability (S2), an OPC-based sealant based on S2, but containing olivine as a CO_2-sequestering agent (S3), a sealant based on calcium-aluminate cement (S4), and a rock-based geopolymer currently under development for use as a wellbore sealant (S5). These five sealants were specifically selected to cover a wide range of compositions, and to compare different mechanisms for enhancing the long-term integrity of wellbore sealants used in GCS applications. The impact of CO_2 exposure microstructure, chemical composition, and mineralogical composition was assessed through analytical techniques such as SEM with EDS, ICP-OES, and CT-scanning. These impacts were then interpreted in terms of CO_2-ingress, carbonisation, and degradation.

Based on testing with phenolphthalein, carbonation of free $Ca(OH)_2$ had penetrated fully through all sealant samples (12 mm diameter cylinders) already after 4 weeks exposure. However, depths and degrees of microstructural alteration and material degradation at the sample surfaces varied, based on sealant type or composition.

- Reducing sealant porosity and permeability, for an OPC-based sealant (i.e., comparing S1 and S2) did not significantly impact the depth of alteration (densification), though it did reduce the degree of change seen in this zone.
- Reducing sealant porosity and permeability did significantly reduce the depth to which the sealant was degraded due to leaching of Ca^{2+} from the CSH-gel, and subsequent dissolution of the leached gel. This was most notable in the samples exposed to CO_2-saturated water, though differences in degradation were also seen in the samples exposed to wet supercritical CO_2.
- The replacement of a significant part of the OPC binder with olivine in S3 (compared to S2) led to degradation deeper into the sample, but the degree of degradation was less severe. However, clear indications of participation of the (larger) olivine grains in the carbonation process were not observed in this study, but will be addressed in future research
- Developing sealant that is less reactive, and which is less negatively impacted by exposure reactions is another interesting strategy for improving long-term sealant integrity. Sealant S5 (rock-based geopolymer) has been engineered to have low Ca-content, to limit the structural importance of Ca in the cured geopolymer gel. As a result, while Ca-leaching did take place, exposure to CO_2-saturated water only had a limited impact on sealant integrity, while exposure to wet supercritical CO_2 lead to negligible degradation.
- A final option for developing a CO_2-resistant binder is to develop a binder material that is chemically inert when exposed to CO_2 and water. This was achieved using a sealant based calcium aluminate cement (S4), which shows very little to no degradation or reaction upon exposure to CO_2-saturated water or wet supercritical CO_2. However, it should be noted that wellbore integrity loss may result from factors other than chemical degradation of the sealant. When this does take place, a reactive sealant, especially one that can release cations that can bind CO_2 and form a stable carbonate, can be an important mechanism for healing leakage pathways, and maintaining or re-establishing seal integrity.

Funding statement

The CEMENTEGRITY project is funded through the ACT programme (Accelerating CCS Technologies, Horizon2020 Project No 691712). Financial contributions from the Research Council of Norway (RCN), The Netherlands Enterprise Agency (RVO), the Department for Energy Security & Net Zero (DESNZ, UK), and Wintershall DEA are gratefully acknowledged.

CRediT authorship contribution statement

Reinier van Noort: Writing – original draft, Visualization, Validation, Supervision, Project administration, Methodology, Investigation, Funding acquisition, Formal analysis, Data curation, Conceptualization. **Gaute Svenningsen:** Writing – review & editing, Methodology, Investigation, Funding acquisition, Data curation, Conceptualization. **Kai Li:** Writing – review & editing, Visualization, Methodology, Investigation, Formal analysis. **Anne Pluymakers:** Writing – review & editing, Methodology, Funding acquisition, Conceptualization.

Declaration of competing interest

The authors declare the following financial interests/personal relationships which may be considered as potential competing interests:

Reinier van Noort reports financial support was provided by Harbour Energy. Reinier van Noort reports samples were provided by Halliburton. If there are other authors, they declare that they have no known competing financial interests or personal relationships that could have appeared to influence the work reported in this paper.

Acknowledgment

The authors thank Mayank Gupta for carrying out the phenolphthalein tests reported here.

Data availability

Data will be made available on request.

References

Abdoulghafour, H., Gouze, P., Luquot, L., Leprovost, R., 2016. Characterization and modeling of the alteration of fractured class-G Portland cement during flow of CO2-rich brine. Int. J. Greenh. Gas Control 48, 155–170. https://doi.org/10.1016/j.ijggc.2016.01.032.

Abdoulghafour, H., Luquot, L., Gouze, P., 2013. Characterization of the mechanisms controlling the permeability changes of fractured cements flowed through by CO_2-rich brine. Environ. Sci. Technol. 47 (18), 10332–10338. https://doi.org/10.1021/es401317c.

Abid, K., Gholami, R., Choate, P., Nagaratnam, B.H., 2015. A review on cement degradation under CO2-rich environment of sequestration projects. J. Nat. Gas. Sci. Eng. 27, 1149–1157. https://doi.org/10.1016/j.jngse.2015.09.061.

Barlet-Gouédard, V., Rimmelé, G., Goffé, B., Porcherie, O., 2006. Mitigation strategies for the risk of CO2 migration through wellbores. In: IADC/SPE Drilling Conference.

Bjørge, R., Gawel, K., Chavez Panduro, E.A., Torsæter, M., 2019. Carbonation of silica cement at high-temperature well conditions. Int. J. Greenh. Gas Control 82, 261–268. https://doi.org/10.1016/j.ijggc.2019.01.011.

Brothers, L., Palmer, A., Caveny, W., 2006. Cement Compositions with Improved Corrosion Resistance and Methods of Cementing in Subterranean Formations. (United States Patent No. US20040211562A1).

Brunet, J.-P.L., Li, L., Karpyn, Z.T., Kutchko, B.G., Strazisar, B., Bromhal, G., 2013. Dynamic evolution of cement composition and transport properties under conditions relevant to geological carbon sequestration. Energy Fuels 27 (8), 4208–4220. https://doi.org/10.1021/ef302023v.

Carey, J.W., Wigand, M., Chipera, S.J., WoldeGabriel, G., Pawar, R., Lichtner, P.C., Wehner, S.C., Raines, M.A., Guthrie, G.D., 2007. Analysis and performance of oil well cement with 30 years of CO2 exposure from the SACROC Unit, West Texas, USA. Int. J. Greenh. Gas Control 1 (1), 75–85. https://doi.org/10.1016/S1750-5836(06)00004-1.

Carroll, S., Carey, J.W., Dzombak, D., Huerta, N.J., Li, L., Richard, T., Um, W., Walsh, S. D.C., Zhang, L., 2016. Review: role of chemistry, mechanics, and transport on well integrity in CO2 storage environments. Int. J. Greenh. Gas Control 49, 149–160. https://doi.org/10.1016/j.ijggc.2016.01.010.

Celia, M.A., Bachu, S., Nordbotten, J.M., Gasda, S.E., Dahle, H.K., 2005. Quantitative estimation of CO2 leakage from geological storage: analytical models, numerical models, and data needs. In: Rubin, E.S., Keith, D.W., Gilboy, C.F., Wilson, M., Morris, T., Gale, J., Thambimuthu, K. (Eds.), Greenhouse Gas Control Technologies, Greenhouse Gas Control Technologies, 7. Elsevier Science Ltd, pp. 663–671. https://doi.org/10.1016/B978-008044704-9/50067-7.

Chavez Panduro, E.A., Torsæter, M., Gawel, K., Bjørge, R., Gibaud, A., Yang, Y., Bruns, S., Zheng, Y., Sørensen, H.O., Breiby, D.W., 2017. In-situ X-ray tomography study of cement exposed to CO(2) saturated brine. Environ. Sci. Technol. 51 (16), 9344–9351. https://doi.org/10.1021/acs.est.6b06534.

Crow, W., Brian Williams, D., William Carey, J., Celia, M., Gasda, S., 2009. Wellbore integrity analysis of a natural CO2 producer. Energy Procedia 1 (1), 3561–3569. https://doi.org/10.1016/j.egypro.2009.02.150.

Duguid, A., 2009. An estimate of the time to degrade the cement sheath in a well exposed to carbonated brine. Energy Procedia 1 (1), 3181–3188. https://doi.org/10.1016/j.egypro.2009.02.101.

Duguid, A., Scherer, G.W., 2010. Degradation of oilwell cement due to exposure to carbonated brine. Int. J. Greenh. Gas Control 4 (3), 546–560. https://doi.org/10.1016/j.ijggc.2009.11.001.

Gu, T., Guo, X., Li, Z., Cheng, X., Fan, X., Korayem, A., Duan, W.H., 2017. Coupled effect of CO2 attack and tensile stress on well cement under CO2 storage conditions. Constr. Build. Mater. 130, 92–102. https://doi.org/10.1016/j.conbuildmat.2016.10.117.

Hajiabadi, S.H., Khalifeh, M., van Noort, R., 2023a. Multiscale insights into mechanical performance of a granite-based geopolymer: unveiling the micro to macro behavior. Geoenergy Sci. Eng. 231, 212375. https://doi.org/10.1016/j.geoen.2023.212375.

Hajiabadi, S.H., Khalifeh, M., van Noort, R., 2024. Stability analysis of a granite-based geopolymer sealant for CO2 geosequestration: in-situ permeability and mechanical behavior while exposed to brine. Cem. Concr. Compos. 149, 105511. https://doi.org/10.1016/j.cemconcomp.2024.105511.

Hajiabadi, S.H., Khalifeh, M., van Noort, R., Silva Santos Moreira, P.H., 2023b. Review on geopolymers as wellbore sealants: state of the art optimization for CO2 exposure and perspectives. ACS. Omega 8 (26), 23320–23345. https://doi.org/10.1021/acsomega.3c01777.

Hernández-Rodríguez, A., Montegrossi, G., Huet, B., Vaselli, O., Virgili, G., 2017. A study of wellbore cement alteration controlled by CO2 leakage in a natural analogue for geological CO2 storage. Appl. Geochem. 86, 13–25. https://doi.org/10.1016/j.apgeochem.2017.09.010.

IEAGHG. (2011). Effects of impurities on geological storage of CO2. (2011/04).

IPCC, 2022. Contribution of Working Group III to the Sixth Assessment Report of the Intergovernmental Panel on Climate Change. C. U. Press.

Jacquemet, N., Pironon, J., Lagneau, V., Saint-Marc, J., 2012. Armouring of well cement in H2S–CO2 saturated brine by calcite coating – Experiments and numerical modelling. Appl. Geochem. 27 (3), 782–795. https://doi.org/10.1016/j.apgeochem.2011.12.004.

Jacquemet, N., Pironon, J., Saint-Marc, J., 2008. Mineralogical changes of a well cement in various H2S-CO2(-Brine) fluids at high pressure and temperature. Environ. Sci. Technol. 42 (1), 282–288. https://doi.org/10.1021/es070853s.

Khalifeh, M., Saasen, A., Vrålstad, T., Larsen, H.B., Hodne, H., 2016. Experimental study on the synthesis and characterization of aplite rock-based geopolymers. J. Sustain. Cem. Based. Mater. 5 (4), 233–246. https://doi.org/10.1080/21650373.2015.1044049.

Kutchko, B., Lopano, C., Strazisar, B., Hawthorne, S., Miller, D., Thaulow, N., Zhang, L., Guthrie, G., 2015. Impact of oil well cement exposed to H2S saturated fluid and gas at high temperatures and pressures: implications for acid gas injection and Co-sequestration. J. Sustain. Energy Eng. 3 (1), 80–101. https://doi.org/10.7569/jsee.2015.629509.

Kutchko, B.G., Strazisar, B.R., Dzombak, D.A., Lowry, G.V., Thaulow, N., 2007. Degradation of well cement by CO2 under geologic sequestration conditions. Environ. Sci. Technol. 41 (13), 4787–4792. https://doi.org/10.1021/es062828c.

Kutchko, B.G., Strazisar, B.R., Hawthorne, S.B., Lopano, C.L., Miller, D.J., Hakala, J.A., Guthrie, G.D., 2011. H2S–CO2 reaction with hydrated Class H well cement: acid-gas injection and CO2 Co-sequestration. Int. J. Greenh. Gas Control 5 (4), 880–888. https://doi.org/10.1016/j.ijggc.2011.02.008.

Kutchko, B.G., Strazisar, B.R., Huerta, N., Lowry, G.V., Dzombak, D.A., Thaulow, N., 2009. CO2 reaction with hydrated class H well cement under geologic sequestration conditions: effects of flyash admixtures. Environ. Sci. Technol. 43 (10), 3947–3952. https://doi.org/10.1021/es803007e.

Kutchko, B.G., Strazisar, B.R., Lowry, G.V., Dzombak, D.A., Thaulow, N., 2008. Rate of CO2 attack on hydrated class H well cement under geologic sequestration conditions. Environ. Sci. Technol. 42 (16), 6237–6242. https://doi.org/10.1021/es800049r.

Kvassnes, A., Clausen, J.A., 2021. Composition of a Cement Additive Material as an Additive to Cementitious Mineral Admixtures, and Utilized as Latent Hydraulic Binders to Improve the Outcome of Cementitious Products. United States Patent No. US11014851B2.

Laudet, J.-B., Garnier, A., Neuville, N., Le Guen, Y., Fourmaintraux, D., Rafai, N., Burlion, N., Shao, J.-F., 2011. The behavior of oil well cement at downhole CO2 storage conditions: static and dynamic laboratory experiments. Energy Procedia 4, 5251–5258. https://doi.org/10.1016/j.egypro.2011.02.504.

Lende, G., Clausen, J.A., & Kvassnes, A.J. (2021). Evaluation of new innovative cement blend for enhanced CO2 and H2S resistance SPE/IADC International Drilling Conference and Exhibition 2021, https://doi.org/10.2118/204103-MS.

Lende, G., Sørensen, E., Jandhyala, S.R.K., Van Noort, R., 2024, 26-28 June 2024. In: State of the art Test Method to Quantify Progression Rate of Carbonation of Wellbore Sealing Materials SPE Europe Energy Conference and Exhibition. Turin, Italy.

Lesti, M., Tiemeyer, C., Plank, J., 2013. CO2 stability of Portland cement based well cementing systems for use on carbon capture & storage (CCS) wells. Cem. Concr. Res. 45, 45–54. https://doi.org/10.1016/j.cemconres.2012.12.001.

Li, K., Pluymakers, A.M.H., 2024a. Effects of Thermal Cycling on Sealing Ability of Sealant Surrounding Steel Pipe for CCS Applications, 13-16 May 2024. InterPore2024, Qingdao, China.

Li, K., Pluymakers, A.M.H., 2024b. Effects of thermal shocks on integrity of existing and newly-designed sealants for CCS applications. Int. J. Greenh. Gas Control 133, 104103. https://doi.org/10.1016/j.ijggc.2024.104103.

Liteanu, E., Spiers, C.J., 2011. Fracture healing and transport properties of wellbore cement in the presence of supercritical CO2. Chem. Geol. 281 (3), 195–210. https://doi.org/10.1016/j.chemgeo.2010.12.008.

Marini, L., 2007. Chapter 5 - the product solid phases. In: Marini, L. (Ed.), Developments in Geochemistry, Developments in Geochemistry, 11. Elsevier, pp. 79–167. https://doi.org/10.1016/S0921-3198(06)80025-6.

Matteo, E.N., Scherer, G.W., 2012. Experimental study of the diffusion-controlled acid degradation of class H Portland cement. Int. J. Greenh. Gas Control 7, 181–191. https://doi.org/10.1016/j.ijggc.2011.07.012.

Nakano, K., Mito, S., Xue, Z., 2017. Self-sealing of wellbore cement under the CO2 batch experiment using Well composite sample. Energy Procedia 114, 5212–5218. https://doi.org/10.1016/j.egypro.2017.03.1677.

Omosebi, O., Maheshwari, H., Ahmed, R., Shah, S., Osisanya, S., Santra, A., Saasen, A., 2015. Investigating temperature effect on degradation of well cement in HPHT carbonic acid environment. J. Nat. Gas. Sci. Eng. 26, 1344–1362. https://doi.org/10.1016/j.jngse.2015.08.018.

Sterpenich, J., Jobard, E., El Hajj, H., Pironon, J., Randi, A., Caumon, M.-C., 2014. Experimental study of CO2 injection in a simulated injection well: the MIRAGES experiment. Greenh. Gases: Sci. Technol. 4 (2), 210–224. https://doi.org/10.1002/ghg.1389.

Suryanto, B., Starrs, G., Kvassnes, A., 2024. Assessment of bond strength of various cementitious sealants for CCS Well applications. In: Proceedings of Joseph Aspdin 200 International Symposium, Innovations in Binder Technology. Edinburgh.

Todorovic, J., Opedal, N.V., Werner, B., Angelique Clausen, J., Jæger Sweetman Kvassnes, A., 2020. Effect of long-term aging in carbonated brine on mechanical properties of a novel cement system with an expandable agent. In: SPE Norway Subsurface Conference.

UNFCCC, 2015. Paris agreement - United Nations Framework Convention on Climate Change. https://unfccc.int/sites/default/files/english_paris_agreement.pdf.

van Noort, R., Spiers, C.J., Drury, M.R., Kandianis, M.T., 2013. Peridotite dissolution and carbonation rates at fracture surfaces under conditions relevant for in situ mineralization of CO2. Geochim. Cosmochim. Acta 106, 1–24. https://doi.org/10.1016/j.gca.2012.12.001.

van Noort, R., Svenningsen, G., & Li, K. (Submitted). Experimental Study on the Impact of H2S and H2SO4 in CO2 on Five Different Sealant Compositions Under Conditions Relevant for Geological CO2-storage. Geoenergy Science and Engineering.

Walsh, S.D.C., Mason, H.E., Du Frane, W.L., Carroll, S.A., 2014. Experimental calibration of a numerical model describing the alteration of cement/caprock interfaces by carbonated brine. Int. J. Greenh. Gas Control 22, 176–188. https://doi.org/10.1016/j.ijggc.2014.01.004.

Wigand, M., Kaszuba, J.P., Carey, J.W., Hollis, W.K., 2009. Geochemical effects of CO2 sequestration on fractured wellbore cement at the cement/caprock interface. Chem. Geol. 265 (1), 122–133. https://doi.org/10.1016/j.chemgeo.2009.04.008.

Wolterbeek, T.K.T., Hangx, S.J.T., Spiers, C.J., 2016. Effect of CO2-induced reactions on the mechanical behaviour of fractured wellbore cement. Geomech. Energy Environ. 7, 26–46. https://doi.org/10.1016/j.gete.2016.02.002.

Xiao, T., McPherson, B., Bordelon, A., Viswanathan, H., Dai, Z., Tian, H., Esser, R., Jia, W., Carey, W., 2017. Quantification of CO2-cement-rock interactions at the well-caprock-reservoir interface and implications for geological CO2 storage. Int. J. Greenh. Gas Control 63, 126–140. https://doi.org/10.1016/j.ijggc.2017.05.009.

Zhang, L., Dzombak, D.A., Nakles, D.V., Hawthorne, S.B., Miller, D.J., Kutchko, B., Lopano, C., Strazisar, B., 2014a. Effect of exposure environment on the interactions between acid gas (H2S and CO2) and pozzolan-amended wellbore cement under acid gas co-sequestration conditions. Int. J. Greenh. Gas Control 27, 309–318. https://doi.org/10.1016/j.ijggc.2014.06.030.

Zhang, L., Dzombak, D.A., Nakles, D.V., Hawthorne, S.B., Miller, D.J., Kutchko, B.G., Lopano, C.L., Strazisar, B.R., 2014b. Rate of H2S and CO2 attack on pozzolan-amended class H well cement under geologic sequestration conditions. Int. J. Greenh. Gas Control 27, 299–308. https://doi.org/10.1016/j.ijggc.2014.02.013.

Zhang, M., Bachu, S., 2011. Review of integrity of existing wells in relation to CO2 geological storage: what do we know? Int. J. Greenh. Gas Control 5 (4), 826–840. https://doi.org/10.1016/j.ijggc.2010.11.006.